

1 **RESPONSE TO REVIEWER COMMENTS. REVIEWER #1**
2

3 We thank the reviewer for their comments, which we have used to clarify the research strategy and
4 generally improve the manuscript.

5
6 Comment-1: Samples are taken in clusters covering only 12 fields in the study area (containing
7 presumably a few 102 fields), with rather a poor spatial distribution. This will most probably affect
8 the distribution of the data in the multi-dimensional space, and hence, do not cover enough the
9 associated landscape complexity within the study area. These 2 concerns (poor spatial distribution
10 and poor distribution in multi-dimensional space) are a major problem when the model is used for
11 extrapolation / predicting pixels elsewhere in study area, i.e. outside the variable range covered by
12 the calibration dataset.

13
14 Response-1: Although the samples are grouped spatially in fields for logistical reasons, they were
15 carefully located to capture the distribution of conditions across the feature space of the agricultural
16 fields. Specifically, the samples include the variety of parent materials in the study area, form
17 transects across topographic positions, as well as cover regional highs and lows. If the modelling
18 technique relied on spatial autocorrelation, such as with kriging, the spatial position of these
19 samples would indeed have been a problem. However, because the modelling method uses spatial
20 regression, which relies on the principle of spatial association, the important space to cover was the
21 feature space. Therefore, the samples were taken to encompass the variable range of the agriculture
22 fields as best could be determined prior to sampling. Notably, only agricultural fields were sampled
23 and thus non-agricultural areas are masked out of prediction maps because they were outside the
24 variable range covered by the calibration dataset. Text has been added to emphasize these points.

25
26 Comment-2: As a consequence, it's quite possible that the differences in SOC stock maps between
27 the two methods are more the consequence of the fact that the 2 modelling approaches (i.e. direct
28 versus indirect) are reacting differently on this shortcoming (inappropriate multidimensional data
29 cover) then it is actually reflecting a real difference in model output just/purely caused by the fact
30 that 2 different approaches were used.

31
32 Response-2: We understand this concern, but consider the variables used to calculate the SOC stock
33 (indirect) and the SOC stock itself (direct) to be intertwined due to their definitional relationship.
34 Because of this relationship, covering the feature space of one approach increases the probability
35 that the feature space of the other approach is also covered.

36
37 Comment-3: Finally, it's clear how the authors calculated errors on SOC stocks by using classical
38 error propagation techniques for individual pixels (i.e. for both the direct and the indirect method
39 (including error predictions on components)), but it's not clear if/how spatial autocorrelation was
40 taken into account when mapping these errors. It's important to integrate this effect of spatial
41 autocorrelation in order to make a fair comparison between the error maps obtained by the two
42 methods.

43
44 Response-3: Spatial autocorrelation was used in the grouping of rule condition zones, on which error
45 estimations are applied. Spatial autocorrelation minimizes how different unsampled areas within a
46 condition zone could be from the sampled locations. This closely resembles the approaches of
47 Shrestha and Solomatine (2006) and Malone et al. (2006) for taking autocorrelation into account
48 when mapping estimated errors from spatial regression models.

52 **RESPONSE TO REVIEWER COMMENTS. REVIEWER #2**

53
54 We thank the reviewer for their comments and suggestions for improving the paper. The following is
55 our response to the specific comments.

56
57 Comment-1: I wonder about the effect of the 10 closely-paired samples...in addition to ensuring the
58 estimated errors capture random variation, could it induce a bias towards these sample points?

59
60 Response-1: The closely-paired samples were spread across the feature space, which should help
61 them be representative of the random variation across the spectrum of conditions and minimize
62 emphasis on a particular set of conditions. Some text was added to explain this part of the sampling
63 strategy.

64
65 The Cubist software does have an option for dealing with data sets that are biased towards a
66 grouping of target variable values. Our experimentation with this feature did not produce regression
67 equations or estimated errors that were very different from those produced without that feature
68 activated. This gives us confidence that the closely-paired samples were distributed in a way to not
69 bias the models built.

70
71 Comment-2: I am a little bit worried about the large number of potential predictors in the pool
72 compared to the number of data on the target variable (117). I appreciate that the authors use the
73 discussion to suggest explanations of why particular predictors were selected, and thus partly
74 validate their selection, but am still not totally convinced that the same could not be done even with
75 junk data and this many potential predictors. I wonder if some acknowledgement of the potential of
76 data-mining software to overfit should be included and commented on. I don't think Cubist does
77 anything to deal with the size of predictor pool (in a multiple hypothesis testing kind of way): : : a
78 comment on this issue could be useful.

79
80 Response-2: Text has been added to provide more detail about how we used Cubist to reduce the
81 predictor pool. Specifically, multiple passes were used so that the final models were built from
82 predictor pools equal to the size of the sets used in the models (3-19 predictors divided between
83 multiple rules). This is explained in greater detail in the referenced paper Miller et al. (2015).

84
85 Comment-3: As you state in the methods section, for the propagation of error in the indirect
86 approach, the variances and covariances should be those of the residuals from the fitted models, not
87 of the data themselves. It seems that this is what was done, but lines 5 and 6 of page 770 made me
88 wonder if the variances and covariances of the raw data had been used. Could you clarify this, as this
89 could be an alternative explanation of the larger uncertainties resulting from the indirect approach?

90
91 Response-3: The text has been corrected to specify the use of the residual's covariance.

92
93 Comment-4: Define f in Equations 2 and 3, and explain exactly what $|f|$ is.

94
95 Response-4: $|f|$ is now defined with an explanation for why it is used. Equation 3 was also corrected.

96
97 Comment-5: In the cross validation (Table 5), I am not sure why the results for predictions of SOC
98 stock by the indirect approach are omitted. I think the table should include these.

99
100 Response-5: Cross-validation was only conducted on the products of the Cubist models themselves.
101 To cross-validate the SOC stock predictions from the indirect approach would be the cumulative
102 cross-validations of the component models. We argue that cross-validations only offer a measure of

103 the models' robustness (how much it would change if different points were used), but does not
104 measure the quality of the best model's performance. For these reasons, calculating a cross-
105 validation of the SOC stock from cross-validations of the component models would be intensive
106 without a large gain in information.

107
108 Comment-6: I think it would also be good to provide some validation of the uncertainties...I
109 appreciate the difficulties of validating with a small, clustered dataset such as this, but I think it
110 would be worth including some measure of the adequacy of uncertainty assessment in the cross
111 validation. One possibility is the mean of the theta-statistic, which should be close to 1 (see e.g. Lark,
112 RM. 2000. A comparison of some robust estimators of the variogram for use in soil survey. European
113 Journal of Soil Science, 51, 137-157).

114
115 Response-6: We contend that the cross-validation statistics are not really a validation of the model
116 based on all of the sample points, especially for MLR models of soil systems. For this reason, our
117 focus in this paper is to compare the results of the two modelling approaches with each other.
118 Nonetheless, the change in the MAE between the models used (based on all points) and the cross-
119 validation models are compared. Additional text has been added to point out that the stability of the
120 MAEs suggests that the estimated uncertainties are also robust.

121
122 Comment-7: It is quite interesting that although the ME for all subsoil component variables was <1,
123 the resulting predictions of SOC stock gave a ME of 1.67. This is worth commenting on in Section
124 3.1.1.

125
126 Response-7: We agree this is an intriguing result and text has been added to section 3.1.1. to
127 highlight it.

128
129 Comment-8: I think that the residuals for all variables are assumed normal...however, depending on
130 the dataset, it may be more appropriate to model log SOC % as normally distributed. Some comment
131 about this, and about the effect that this could have on predictions and uncertainties in the indirect
132 approach could be useful.

133
134 Response-8: This is indeed an important point. Text, along with a table of residual skewness
135 coefficients, has been added to describe the distribution of the residuals and their potential effect
136 on the results.

137
138 Comment-9: Is a conservative estimate of the spatial distribution the best thing? The most
139 conservative would be to use the mean across the entire study area, but this would not be very
140 useful. I am not sure whether the paper is recommending that the more conservative approach
141 should be used, or just saying that the direct approach is more conservative than the indirect
142 approach.

143
144 Response-9: Recognizing that different situations will have different needs, we were careful to chose
145 the term 'conservative' to avoid judging which approach may be best for a given set of goals or
146 purpose. Specifically, sometimes representing variation can be more useful than minimizing the
147 amount of error, and vice versa. A sentence has been added to the conclusions to emphasize this
148 point.

149
150 Comment-10: What exactly is meant by the 'spatial association approach'?

151
152 Response-10: Spatial association is a term parallel to spatial autocorrelation. Like the specific
153 method of kriging is often described when applying a spatial autocorrelation approach, the term

154 spatial regression is a popular method for applying the concept of spatial association. We use the
155 term spatial association frequently to emphasize the difference between our study and a similar
156 study that compared different spatial autocorrelation methods. Additional text has been added to
157 clarify spatial association for those who may not be familiar with the term.

158

159 Comment-11: Were all soil profiles deeper than 2 m?

160

161 Response-11: Thank you for catching this omission. Indeed field logistics prevented the full 2 m from
162 being sampled for some of the profiles and some assumptions needed to be made. Text explaining
163 this has been added.

164

165 Comment-12: Page 767, sentence starting on line 27: 'correlation...of $R^2 = 0.59$ '. Correlation should
166 be measured by r , not R^2 ...reword this sentence.

167

168 Response-12: Wording has been corrected.

169

170 Comment-13: Page 768, line 6: direct $R^2 = 0.14$, but in Table 4 is 0.19...is this correct?

171

172 Response-13: The typographical error has been fixed.

173

174 Comment-14: Figures 2, 3 and 4: I am not sure that the hillshade effect helps. I found it difficult to
175 distinguish between the effect of the hillshade and the SOC stock differences. I would suggest
176 removing this effect.

177

178 Response-14: Agreed. The hillshade effect has been removed from the respective figures.

179

180 **MARKED-UP MANUSCRIPT VERSION**

181 **Comparison of spatial association approaches for landscape mapping of soil organic carbon stocks**

182 Bradley A. Miller*, Sylvia Koszinski, Marc Wehrhan, and Michael Sommer

183 Leibniz Centre for Agricultural Landscape Research (ZALF) e.V., Institute of Soil Landscape Research,

184 Eberswalder Straße 84, 15374 Müncheberg, Germany

185 *Corresponding author

186 Email addresses: miller@zalf.de (B.A. Miller), skoszinski@zalf.de (S. Koszinski), wehrhan@zalf.de (M.

187 Wehrhan), sommer@zalf.de (M. Sommer)

188

189 **Abstract**

190 The distribution of soil organic carbon (SOC) can be variable at small analysis scales, but

191 consideration of its role in regional and global issues demands the mapping of large extents. There

192 are many different strategies for mapping SOC, among which are to model the variables needed to

193 calculate the SOC stock indirectly or to model the SOC stock directly. The purpose of this research is

194 to compare direct and indirect approaches to mapping SOC stocks from rule-based, multiple linear

195 regression models applied at the landscape scale via spatial association. The final products for both

196 strategies are high-resolution maps of SOC stocks (kg m^{-2}), covering an area of 122 km^2 , with

197 accompanying maps of estimated error. For the direct modelling approach, the estimated error map

198 was based on the internal error estimations from the model rules. For the indirect approach, the

199 estimated error map was produced by spatially combining the error estimates of component models

200 via standard error propagation equations. We compared these two strategies for mapping SOC

201 stocks on the basis of the qualities of the resulting maps as well as the magnitude and distribution of

202 the estimated error. The direct approach produced a map with less spatial variation than the map

203 produced by the indirect approach. The increased spatial variation represented by the indirect
204 approach improved R^2 values for the topsoil and subsoil stocks. Although the indirect approach had a
205 lower mean estimated error for the topsoil stock, the mean estimated error for the total SOC stock
206 (topsoil + subsoil) was lower for the direct approach. For these reasons, we recommend the direct
207 approach to modelling SOC stocks be considered a more conservative estimate of the SOC stocks'
208 spatial distribution.

209 *Keywords:* digital soil mapping, organic carbon, spatial association, estimated error, uncertainty

210

211 Highlights

212 1. Spatial association methods for mapping SOC stock directly and indirectly were compared.
213 2. Data mining produced models that could be interpreted by expert knowledge.
214 3. The indirect approach map had greater spatial variation and higher R^2 values.
215 4. The direct approach map had less spatial variation and a lower total estimated error.

216 **1. Introduction**

217 The storage of carbon in soil is a critical point of information for several environmental issues.
218 Globally, soil carbon, which is about 60% organic carbon, accounts for 3.3 times more carbon than
219 that found in the atmosphere (Lal, 2004). The high amount of carbon stored in the soil, makes soil
220 carbon an important factor for understanding the carbon cycle and dynamics influencing global
221 climate change (Grace, 2004; Johnston et al., 2004; Powlson et al., 2011). In addition, higher
222 concentrations of soil organic carbon (SOC) are associated with better water storage capacity,
223 regulation of nutrients, and stabilization of soil aggregates resulting in improved soil structure and
224 resistance to erosion (Neemann, 1991; Angers and Carter, 1996; Rawls et al., 2003; Snyder and
225 Vazquez, 2005; Johnston et al., 2009; Kay, 1998; Wilhelm et al., 2004). Each of these factors has
226 important roles in issues of water management and crop productivity.

227 Although SOC management has far reaching implications, the distribution of SOC is highly
228 variable and dynamic at the field-scale (Cambardella et al., 1994; McBratney and Pringle, 1999;
229 Walter et al., 2003; Kravchenko et al., 2006b; Simbahan et al., 2006). Differing conditions, such as
230 hydrology or management practices, greatly impact the SOC content (Kravchenko et al., 2006a). The
231 combination of global implications and high spatial variability make high-resolution maps of SOC for
232 large extents desirable for both policy decisions and land-owner response. This situation creates the
233 need to accurately and efficiently assess the spatial distribution of SOC stocks at a high-resolution.
234 High-resolution mapping captures information essential for assessing field-specific conditions, which
235 can later be aggregated as need to provide summary information.

236 Many studies have tested a variety of strategies for predicting the spatial distribution of SOC
237 (Minasny et al., 2013 and references therein). The various studies on SOC mapping have analyzed
238 different soil depths, which has large implications for the consideration of the complete SOC stock
239 (Richter and Markewitz, 1995; Batjes, 1996; Jobbágy and Jackson, 2000; Sombroek et al., 2000;
240 Schwartz and Namri, 2002; Meersmans et al., 2009). For example, some have focused on spatially
241 modelling the topsoil to depths of 20-30 cm (e.g. Ungaro et al., 2010; Zhang et al., 2010; Martin et

242 al., 2011). Other variations of strategies for digital SOC mapping differ in which variables are
243 modelled in order to predict SOC. For instance, some studies have modelled the SOC stock (e.g. kg
244 m⁻², T ha⁻¹, kg m⁻³) directly (Simbahan et al., 2006; Lufafa et al., 2008; Nyssen et al., 2008; Mishra et
245 al., 2010; Phachomphon et al., 2010; Kempen et al., 2011), while others have separately modelled
246 the variables needed to calculate the SOC stock and then combined them (Grimm et al., 2008; Khalil
247 et al., 2013; Lacoste et al., 2014). The usual component variables are total bulk density (BD), particles
248 > 2 mm (SK), SOC concentration (SOC%), and stock thickness (H), which are then combined by:

249
$$SOC_{stock} = \left(\frac{SOC\%}{100} \right) * (BD * 1000) * \left(\frac{100-SK}{100} \right) * H \quad (1)$$

250 where, SOC_{stock} is in kg m⁻², SOC% is in percent, BD in g cm⁻³, SK in percent, and H in m.

251 Irrespective of the approach used, an important output of digital soil mapping is a measure of
252 uncertainty. Orton et al. (2014) compared uncertainties resulting from directly modelling the SOC
253 stock (direct = calculate-then-model) with modelling component variables for calculating the SOC
254 stock (indirect = model-then-calculate), based on geostatistical approaches that rely on spatial
255 autocorrelation. In the present study, we made a similar assessment for rule-based, multiple linear
256 regression (MLR) models, which rely on spatial association.

257 With the spatial association (i.e. spatial regression) approach to soil mapping, the empirical
258 model error can be transferred along with the model itself (Lemercier et al., 2012). For digital soil
259 mapping, Malone et al. (2011) adapted the Shrestha and Solomatine (2006) approach for empirically
260 summarizing model error and extending that information to prediction areas. In those previous
261 studies, areas expected to have similar errors were grouped by cluster analysis. Because similar sites
262 are already grouped together in rule-based, MLR models, the estimated errors can be applied to the
263 areas meeting the same rule conditions and thus mapped. The ability to map predictions of soil
264 properties and the confidence in those predictions via spatial association is important for landscape
265 to national extents because of the common limitation of sampling density (Martin et al., 2014).

266 The purpose of this study was to compare the maps of SOC stocks produced from direct and
267 indirect modelling approaches, using rule-based MLR. The resulting maps were compared in terms of
268 their predicted spatial patterns, coefficient of determination (R^2), as well as the magnitude and
269 spatial distribution of the estimated errors. The predictors selected for the models via the data
270 mining procedure were evaluated in the context of known landscape processes. In addition, the
271 separate assessment of topsoil and subsoil stocks tested the models' ability to predict SOC storage at
272 depths to two meters.

273 **2. Methods**

274 *2.1. Study Area and Sampling*

275 A dominantly agricultural area located near Wulfen, Saxony-Anhalt, Germany, which has been
276 examined by several previous studies (Selige et al., 2006; Brenning et al., 2008; Kühn et al., 2009;
277 Migdall et al., 2009), was selected for this research. The mapping area extends from 11.86°N,
278 51.74°E to 11.96°N, 51.90°E (Figure 1), covering a total area of 122 km². The landscape includes
279 hummocky till plain, outwash plain, loess, and a broad floodplain (Königlich Preußische Geologische
280 Landesanstalt, 1913a, b). The study area is dominated by Calcaric Cambisols and Luvic Phaeozems,
281 while the depressional area in the floodplain is primarily Dystric Gleysols (European Commission,
282 2014). Between 2005 and 2006, 117 locations were sampled from a variety of landscape positions in
283 12 different agricultural fields, covering the known feature space for agricultural land in this area.
284 Because all models were calibrated and validated on these samples, evaluation of the resulting maps
285 focused on areas with similar land-use (i.e. water bodies and urban areas excluded). Ten of the
286 sample points, also spread across the feature space, were of repeated locations (within 2 m of
287 original), which helped to insure that random error was reflected in the assessment of estimated
288 error.

289 Soil horizons identified in the field were sampled at each sampling location. To avoid biases from
290 horizon classifications and to focus on the two major process zones for SOC, the soil profile of two

291 meters was divided into topsoil and subsoil stocks. The division was defined by the largest decrease
292 in SOC%, as determined by lab analysis, between field identified horizons. Not all profiles were able
293 to be sampled to the full depth of two meters. In those cases, the properties of the sampled subsoil
294 were assumed to be representative of the remaining depth. Data for the horizons within each stock
295 were combined using a thickness-weighted mean, as appropriate. Descriptive statistics for these
296 observation points are provided in Table 1.

297 *2.2. Modelling*

298 Models for each of the target variables were generated using the Cubist 2.08 software (Quinlan
299 1992, 1993, 1994). Previous studies have demonstrated the utility of this tool for digital soil mapping
300 (Bui et al. 2006; Minasny and McBratney, 2008; Adhikari et al., 2013; Lacoste et al., 2014). Cubist
301 uses a data mining algorithm to build two-tiered models. The top level consists of a series of
302 conditional rules that can utilize both continuous and categorical predictors. For each rule, a MLR
303 equation is produced for predicting the target variable. Cubist's process for selecting predictors and
304 building the models is described in Quinlan (1993) and Holmes et al. (1999) and will not be repeated
305 here. One advantage of this approach is the interpretability of the produced model, which allows the
306 modeler to assess relationships between the model and physical processes (Bui et al., 2006).

307 The results of the data mining process are dependent upon the predictors made available to the
308 data mining software. For this reason, we used the large predictor pool method described by Miller
309 et al. (2015) to identify the optimal models for each of the respective target variables. That method
310 includes a multiple pass test, which reapplies the Cubist algorithms to the limited pool selected by
311 the previous run. This helps to insure that the selected predictors have been optimally reduced by
312 the Cubist software, decreasing the concern of overfitting. The predictor pool for this study included
313 410 base maps covering the full extent of the study area (Table 2). These base maps consisted of a
314 legacy geologic map, a variety of remote sensing/spectral products, and digital terrain analysis
315 (DTA). The spectral products ranged from four bands of Ikonos data to a variety of Landsat data

316 collected at different times in 2006. DTA was conducted on a 2 m resolution, digital elevation model
317 (DEM), created from LiDAR data that was also collected in 2006. The DTA base maps included land-
318 surface derivatives based on a wide range of analysis scales (a-scales) and a suite of hydrologic
319 indicators. Land-surface derivatives were calculated in GRASS 6.4.3 (Geographic Resources Analysis
320 Support System, grass.osgeo.org) and ArcGIS 10.1 (www.esri.com/software/arcgis). Hydrologic
321 indicators were calculated using SAGA 2.1.0 (System for Automated Geoscientific Analysis,
322 <http://www.saga-gis.org/en/index.html>).

323 The predictors selected by the Cubist software were then used as base maps to generate maps
324 of SOC_{stock}. Using the raster calculator in ArcGIS 10.1, the base maps were combined according to the
325 MLR equations produced by Cubist. When base maps of different resolutions were combined, the
326 finest resolution was maintained. The respective MLR equations were only applied in the areas that
327 met the conditions of the Cubist model's first tier. The first experimental approach used this method
328 to directly map SOC_{stock} from the SOC_{stock} calculated at each sample point. The second experimental
329 approach used this method to map each of the component variables. These modelled variables were
330 then used as base maps to create a SOC_{stock} map. The raster calculator was then again used to
331 combine the component variables, but this time according to equation 1. For both experimental
332 approaches, the topsoil and subsoil were mapped separately. After the respective SOC_{stock} maps
333 were produced, they were added together to create total SOC_{stock} maps.

334 Within the extent of the study area, there were a few areas with conditions outside the range
335 observed in the point samples. In these limited cases, extreme predictor values produced model
336 predictions of target variables either far below or above the ranges observed for the respective
337 target variables. To address this issue, spatial predictions were limited to be within 10% of the
338 observed target variable minimum and maximums.

339 *2.3. Propagation of Error*

340 For each of the model rules, estimated error was calculated based on the internal fit of the MLR
341 to the data classified within that rule. This estimation provided a measure for the respective
342 uncertainty under each rule. The conditions for the respective rules were used to spatially classify
343 the base maps, thus allowing the estimated errors to be mapped. Measurement error, positional
344 error, and limitations of the model to predict the target variable were all empirically encapsulated by
345 the estimated error.

346 When the target variable was the end product, the uncertainty was simply represented by the
347 estimated error. However, when multiple variables were modelled and subsequently used to
348 calculate the final product, the estimated errors of the component variables propagated through the
349 combination of those variables in the function. In order to map estimated error for the indirect
350 approach of modelling SOC_{stock}, estimated error maps were produced for each of the component
351 variables. These error estimation maps were then combined using standard equations for
352 propagation of error (Mardia et al., 1979; Taylor, 1997; Weisstein, 2014). Although potentially biased
353 by the approximation to a first-order Taylor series expansion, simplified equations for error
354 propagation are more practical and are regularly used in engineering and physical science
355 applications (Goodman, 1960; Ku, 1966). Because covariance between variables has the potential to
356 impact the estimation of SOC_{stock} (Panda et al., 2008; Goidts et al., 2009), we did not assume the
357 variables were independent. The observed residual covariance was thus used to modify the
358 estimated error within the standard equations for propagation of error by multiplication,

$$359 \sigma_f \approx |f| \sqrt{\left(\frac{\sigma_A}{A}\right)^2 + \left(\frac{\sigma_B}{B}\right)^2 + 2 \frac{cov_{AB}}{AB}} \quad (2)$$

360 and by addition,

$$361 \sigma_f \approx \sqrt{\sigma_A^2 + \sigma_B^2 + 2cov_{AB}} \quad (3)$$

362 where f is the result of the original function (to convert from relative to estimated error), A and B are
363 the real variables, with estimated errors σ_A and σ_B , and their residuals' covariance cov_{AB} . In order to

364 calculate a predicted relative error (e.g. $\frac{\sigma_A}{A}$) at unsampled locations, the predicted variable was
365 assumed to accurately represent the variable's magnitude.

366 Locations with small ratios between estimated error and predicted values together with large,
367 negative covariances had the potential to produce a calculation taking the square root of a negative.
368 This issue was addressed by not considering the covariance in those limited circumstances. While
369 this solution may have led to an overestimation of error, it provided a means to mathematically
370 calculate estimated error without declaring it to be zero.

371 **3. Results**

372 *3.1. Models*

373 *3.1.1. Model building and fitting performance*

374 Explicit models were obtained for each of the component variables needed to calculate SOC_{stock}
375 indirectly and for predicting SOC_{stock} directly. Models for predicting component variables used a
376 higher quantity of predictors for each of the respective models than the direct modelling approach
377 (Table 3). With the exception of SOC%, the models for component variables included a combination
378 of DTA and spectral variables. The SOC% models relied solely on DTA predictors for both stocks, but
379 with additional spatial partitioning by geologic map units for the topsoil model. The models for
380 directly predicting the SOC_{stock} used only three DTA predictors for the topsoil and only four Landsat
381 predictors for the subsoil.

382 Fitting performances for the component variable models were better than the fitting
383 performances for the direct modelling of SOC_{stock} (Table 4). For the component variables, R² values of
384 subsoil models were only slightly less than the topsoil models. SOC% was the exception by having the
385 lowest fitting performance for the subsoil stock (R² = 0.55), while the model for the SOC% topsoil was
386 able to fit observations with an R² of 0.86. However, it was the aim of this research to examine if the
387 performance of the models was maintained through the calculation of SOC_{stock}.

388 Comparison of the SOC_{stock} predictions by the indirect approach to observed values showed
389 better performance for the topsoil stock ($R^2 = 0.73$) than for the subsoil stock ($R^2 = 0.34$). Fitting
390 performance for directly modelling SOC_{stock} showed the same pattern, but was lower than the
391 indirect approach for both stocks. Analysis of the direct approach's ability to fit observed values
392 yielded an R^2 of 0.58 for the topsoil and 0.14-19 for the subsoil.

393 In general, calculated model efficiencies (ME) showed that the respective models reduced the
394 mean absolute error (MAE) to about half the MAE that would result from simply using the mean of
395 all points as the prediction. The SOC_% model for the topsoil improved upon the mean model more
396 than the other MLR models with a ME of 0.34. However, an intriguing result is the lack of model
397 efficiency for the indirect modelling of the subsoil's SOC_{stock}. Despite the component models all
398 having MEs well below one, the indirect approach did not improve upon the mean model for
399 predicting the subsoil SOC_{stock}. Although the ME of the direct model for subsoil SOC_{stock} was also not
400 as good as the other models, it was still an improvement over the mean model.

401 3.1.2. Model Robustness

402 It is common for digital soil mapping models to be evaluated by cross-validation procedures.
403 However, in the context of this study, the meaning of such an analysis has less utility. Higher sample
404 density increases the robustness of the model (Minasny et al, 2013); thus the popularity of cross-
405 validation procedures over independent validation procedures in order to maintain more points in
406 the calibration set. However, the model generated for each cross-validation run is different because
407 of differences in calibration sets. The performance of each run is dependent on the randomly
408 selected calibration points' ability to represent the variation in the remaining validation points. For a
409 simple data trend, a single outlier would have minimal effect because only the runs in which it is
410 included in the validation set – and not used in calibrating the model – would have lower
411 performance values. However, in a complex landscape where similar soil properties can result from
412 different combinations of factors, the concept of an outlier has many more dimensions (Johnson et

413 al., 1990; Phillips, 1998). A point with a similar value can be an outlier by being a product of a
414 different set of factors. In other words, the problem of induction continues to apply in predictive soil
415 mapping. Further, in the context of error propagation, the error estimation from the actual model
416 used seems more appropriate than the mean of error estimations from a series of less robust
417 models.

418 Nonetheless, the models in this study were cross-validated using the k-fold method with 10
419 iterations. The R^2 was naturally reduced in the cross-validation analysis, but the ~~mean absolute error~~
420 ~~(MAE)~~ was not as severely affected (Table 5). The R^2 values for the respective models all decreased
421 greatly in the cross-validation, except for the topsoil SOC% and the subsoil SOC_{stock} models. The
422 subsoil SOC_{stock} model already had a low R^2 value for the internal fit. In contrast, the MAEs for the
423 cross-validation of the models were not increased enough to present a practical problem. The
424 relative stability of the MAEs also suggests that the estimated uncertainties are also robust. For
425 example, the MAE for both stocks of BD only increased 0.03 g cm⁻³. Also, the MAE for SOC% only
426 increased 0.13% and 0.03% for the topsoil and subsoil, respectively. Similarly, the MAE for the direct
427 SOC_{stock} model increased 0.67 kg m⁻² and 0.05 kg m⁻² for the topsoil and subsoil, respectively. The
428 MAE for the models of stock H and SK did increase more in cross-validation. However, they had a
429 minor impact on the indirect modelling of SOC_{stock}. The increase of 5.9 cm for the topsoil H MAE was
430 only a shift of the depth estimated by topsoil or subsoil models. The larger MAE for SK was more of
431 an issue for the subsoil. However, the majority of the samples had SK below 5%, leaving most of the
432 error due to the difficulty in predicting the limited areas of high SK. While it was possible that a
433 different sampling design could have improved the R^2 values for cross-validation, they are not always
434 practical for landscape-scale mapping.

435 *3.1.3. Comparison with previous studies*

436 It is difficult to compare results between SOC mapping studies due to differences in study areas
437 and strategies for defining SOC_{stock} (i.e. map extent and resolution, sampling density, and

438 consideration of depth). Further, the differences between and variability within methods for
439 estimating component variables for calculating SOC_{stock} can have a large impact on results, especially
440 bulk density (Liebens and VanMolle, 2003; Schrumpf et al., 2011) and SOC% (Lowther et al., 1990;
441 Soon and Abboud, 1991; Sutherland, 1998; Bowman et al., 2002). Also, because model performance
442 is dependent upon the provided predictors, results of different studies can vary based on the
443 predictors available to and derived by the modeller (Miller et al., 2015). However, because the area
444 in this study has been used for several previous studies, some comparisons between methods can be
445 made.

446 Kühn et al. (2009) examined many of the same samples used in this study and found a
447 correlation-coefficient of determination between soil electrical conductivity and soil organic matter
448 to a 1 m depth (kg m⁻²) of R² = 0.59. Although a slightly different calculation, that correlation
449 coefficient of determination is similar to this study's direct model of topsoil SOC_{stock} (R² = 0.58),
450 which used three DTA predictors. However, for the topsoil, the indirect approach in this study
451 produced a SOC_{stock} model with less estimated error and an R² of 0.73. The Kühn et al. (2009) study
452 usually included depths that this study defined as subsoil, where the models in this study did not
453 perform as well (direct R² = 0.4419, indirect R² = 0.34).

454 For the same area as this study, Selige et al. (2006) compared MLR and partial least-square
455 regression for predicting SOC% from hyperspectral data with a 6 m spatial resolution. Although the
456 study by Selige et al. (2006) utilized a higher spectral resolution, the MLR models produced by both
457 that study and the present study had R² of 0.86 for the topsoil SOC%. In the present study, Cubist was
458 able to compensate for the limited spectral information by utilizing several DTA predictors that were
459 available at a high spatial resolution.

460 3.2. SOC_{stock} maps

461 Application of the obtained models and aggregation of the component variable maps by
462 equation 1 produced maps of predicted SOC_{stock} for the topsoil and subsoil (Figures 2 and 3). The
463 respective topsoil and subsoil maps were added together to produce a total SOC_{stock} map to a depth
464 of 2 m (Figure 4). Although some field boundaries were observed, the dominant pattern appeared to
465 be associated with terrain features. This interpretation was supported by the number of DTA
466 predictors selected by Cubist for many of the models. However, it would not have been safe to
467 assume this pattern from the list of selected predictors alone. Certain predictors (i.e. spectral data
468 reflecting land use patterns) could have dominated calculations without being the most frequently
469 selected category of predictors.

470 The map derived from the direct approach for modelling the topsoil SOC_{stock} emphasizes
471 drainageways. Whereas the map derived by the same approach for the subsoil SOC_{stock} reflects more
472 patterns of land use, especially in the uplands in the southern part of the study area. The topsoil
473 SOC_{stock} map based on the indirect approach has similar overall patterns to the direct approach's
474 map. However, both the topsoil and subsoil maps produced by the indirect approach display greater
475 spatial variation.

476 Patterns in the topsoil SOC_{stock} map, based on the indirect approach, mostly coincide with terrain
477 features, but do contain some transitions that align with field boundaries. The corresponding map
478 for the subsoil reflects patterns of microtopography and slope gradient. Larger values for the subsoil
479 SOC_{stock} are predicted by the indirect approach for local lows in elevation (smaller a-scales).
480 Predictions of larger subsoil SOC_{stock} on steeper slopes result from the modelling of thinner topsoil
481 stocks in these areas and the consistent calculation of a 2 m profile. Consequently, the subsoil is
482 calculated to be thicker in these areas, substantially increasing the subsoil SOC_{stock} prediction
483 compared to other areas of the subsoil.

484 Maps derived by both approaches for the total SOC_{stock} primarily reflected patterns from the
485 topsoil maps because of the higher concentration of SOC that defined the topsoil stock.

486 Nonetheless, modelled storage for the subsoil stock contributed about one-third of the prediction of
487 total SOC_{stock} and recognized additional complexity in the SOC landscape. Despite the greater
488 variation in the indirect approach's prediction of SOC_{stock}, the difference between estimates of total
489 SOC_{stock} by the two approaches were within 5 kg m⁻² for the majority of the map area (Figure 5). Also,
490 the summed SOC_{stock} for the study area was only 6% more for the indirect (1.9 Mt) versus the direct
491 (1.8 Mt) approach. The mean SOC_{stock} estimate for the study area by the direct approach was 14.7 kg
492 m⁻², whereas the indirect approach estimated 15.7 kg m⁻².

493 These aggregated landscape estimates agreed with those made by the Harmonized World Soil
494 Database (HWSD; FAO/IIASA/ISRIC/ISSCAS/JRC, 2012) for this area. The HWSD estimated several soil
495 properties from taxonomic pedotransfer functions for static topsoil (0-30 cm) and subsoil (30-100
496 cm) depth zones. Within the area of the present study, the HWSD has a cell resolution of
497 approximately 765 m. Calculating SOC_{stock} from that data yielded a mean of 8.8 kg m⁻². Assuming the
498 characteristics of the subsoil to 100 cm extended to 200 cm, the mean SOC_{stock} would be 15.3 kg m⁻².

499 *3.3 Error estimations*

500 The mapping of estimated errors based on the conditions of rules generated by Cubist resulted
501 in a spatial representation of uncertainty (Figure 6). In order to calculate the final estimated errors
502 for the indirect approach, estimated errors for models of component variables were combined
503 spatially by equations 3-2 and 43. Due to the known covariance of component variables, the
504 observed covariance of the residuals was included in the calculation of error propagation through
505 the calculation of the total SOC_{stock}. Inclusion of covariance reduced relative error estimates in the
506 topsoil because increases in residuals for BD coincided with decreases in the residuals for percent
507 fine-earth, increases in fine-earth BD residuals coincided with decreases in SOC% residuals, and
508 increases in SOC content (kg m⁻³) residuals coincided with decreases in stock thickness residuals. The
509 influence of covariance was not mostly the same in the subsoil calculations. The exception was a
510 positive covariance between the residuals for modelling BD and the percent fine-earth. With the

511 ~~exception of the covariance between fine earth BD and SOC%, which was very small, subsoil~~
512 ~~covariances were positive. However, overall~~Nonetheless, the covariances were relatively small with
513 respect to the estimated errors and therefore had a minimal impact on the final calculation of
514 estimated error.

515 The application of error estimates based on the full range of predicted values in a rule zone to
516 small values in that zone yielded extremely high relative error values. Although the areal extent for
517 this type of situation was very limited, the issue needed to be addressed in order to maintain the
518 readability of the attribute scale. Therefore relative error was capped at one for the original relative
519 error grids, but not thereafter for the calculation of error propagation.

520 Despite not having as strong of a fitting performance as the indirect approach, the direct
521 approach had lower estimated errors for greater extents of the study area. The mean estimated
522 error for the total SOC_{stock} map derived by the direct approach was 2.81 kg m⁻², compared to 8.17 kg
523 m⁻² for the indirect approach. This behavior in the models may be explained by the negative
524 covariance between the residuals for many of the variables influencing the SOC_{stock}. The observed
525 covariances did reduce the calculation of error through propagation. However, they did not reduce
526 the estimated error for the indirect approach to as low as the estimated error based on the direct
527 modelling approach. It is also useful to note that the residuals for modelling SK and SOC% were had a
528 negative and positive skewed, respectively, for both stocks (Table 6). However, for the
529 residuals effor the final prediction of SOC_{stock}, regardless of approach or stock, only the indirect
530 model for the subsoil had strongly skewed residuals. This suggests that the error for the indirect
531 model of the subsoil SOC_{stock} may have been overestimated.

532 The spatial distribution of model rules was an important factor in the resulting maps' estimated
533 error. The models for the direct approach used fewer rules than the component variable models,
534 resulting in less spatial variation of the estimated error. However, variation in predicted values did
535 introduce additional spatial variation to the mapping of relative error. Nonetheless, the map of

536 relative error from the indirect approach was more complex than that resulting from the direct
537 approach. In addition to using more rules for each model, the combined relative estimated error for
538 the indirect approach was further tessellated by the unique intersections of the different spatial
539 distributions of the rules for each component variable model.

540 **4. Discussion**

541 *4.1. Predictor selection*

542 *4.1.1. Review of relationships between predictors and environmental conditions*

543 Spectral predictors from satellites such as Ikonos and Landsat have most commonly been used
544 to detect characteristics of land use, vegetation, and soil water content (Bannari et al., 1995; Xie et
545 al., 2008). However, they have also been used to detect mineralogy on sparsely vegetated areas
546 (Mulder et al., 2011). Although Ikonos has a finer spatial resolution, it is limited to three bands (band
547 1 = blue, band 2 = green, and band 3 = red) in the visible spectrum, plus a near infrared band (band 4
548 = NIR). Landsat provides additional bands in the shortwave infrared (band 5 = SWIR-1; band 7 =
549 SWIR-2) and thermal infrared (band 6 = TIR). The relative reflectance of a single band can be used to
550 distinguish landscape conditions. For example, the green band can be used to distinguish different
551 vegetation from bare soil. However, combinations of bands - particularly including the red and NIR
552 bands - have been even more useful for distinguishing the spectral signature of different land uses
553 (Richards, 2006) and the condition of the vegetation (Ashley and Rea, 1975; Myneni et al., 1995;
554 Rasmussen, 1998; Daughtry, 2001; Hatfield et al., 2008). Additional use of TIR emission would
555 resemble methods such as the Surface Temperature/Vegetation Index for estimating soil moisture
556 (Bartholic et al., 1972; Heilman et al., 1976; Carlson et al., 1994; Li et al., 2009; Petropoulos et al.,
557 2009). Similarly, use of SWIR wavelengths in concert with red and infrared ~~red~~ bands would be a way
558 of compensating for the changing effect of soil reflection in dry to wet conditions (Huete, 1988;
559 Lobell and Asner, 2002). Relationships between bands in the visible to SWIR range have also been

560 used to predict SOC% and its biochemical composition (Bartholomeus et al., 2008; Gomez et al.,
561 2008; Stevens et al., 2010).

562 Spectral predictors have been used for both classification of discrete phenomenon and
563 quantification of continuous phenomenon on the landscape. Because of the rule-based MLR
564 structure of the Cubist models, spectral predictors used for conditional rules were more likely to be
565 distinguishing discrete features (e.g. vegetation/land use type) than when used within an MLR
566 equation. Continuous features (e.g. vegetation health) were more likely to be represented in MLR
567 equations.

568 DTA predictors in this study were all derived from the LiDAR data for elevation. The land-surface
569 derivatives (e.g. slope gradient, relative elevation) described the surface geometry with which the
570 climate interacts. For example, aspect has been shown to influence the amount of solar insolation a
571 hillslope receives (Hunckler and Schaetzl, 1997; Beaudette and O'Geen, 2009). The surface geometry
572 is also known to direct water flow, which affects erosion processes and groundwater recharge
573 (Huggett, 1975; Zevenbergen and Thorne, 1987). Hydrologic predictors (e.g. flow accumulation,
574 catchment slope) provided additional information about the relative volume and energy that the
575 water flow may have (Moore et al., 1991; Wilson and Gallant, 2000).

576 *4.1.2. Topsoil model predictors*

577 All of the topsoil models generated by Cubist relied on DTA predictors the most. Of those
578 predictors, different a-scales of relative elevation, topographic position index (TPI), and aspect were
579 the most commonly used. With the exception of the direct SOC_{stock} model, every topsoil model also
580 included one or two predictors indicative of flow accumulation (i.e. flow path length, SAGA wetness
581 index, or modified catchment area).

582 Aspect at different a-scales influenced predictions for three of the indirect topsoil models. The
583 Cubist generated model identified decreasing topsoil SOC% on more north facing slopes (155 m a-

584 scale), which corresponds with a potential decrease in plant productivity due to less solar insolation.
585 Aspect (215 m a-scale) was also used to predict higher topsoil BD on south to west facing slopes,
586 especially on topographic (2000 m a-scale) and micro-topographic (20 m a-scale) highs. Additionally,
587 aspect at a variety of a-scales was used to predict decreasing topsoil SK for low TPI areas facing
588 southeast to southwest. Together, these models suggested a pattern of increased erosion and
589 deposition along the southern sides of hillslopes. This type of pattern has been observed before in
590 other landscapes and has been attributed to topo-climatic differences such as exposure to storms,
591 differences in temperature regime, rainfall effectiveness, or vegetation density (Kennedy, 1976;
592 Churchill, 1981; Cuff, 1985; Weaver, 1991).

593 Although DTA parameters dominated the topsoil models, their predictions were often modified
594 by spectral variables. For example, the primary distinction for predicting topsoil H was between low
595 and high relative elevations. Low relative elevations had a mean topsoil H that was about 20 cm
596 thicker than high relative elevations (1,100 m a-scale). Within most MLR equations, however,
597 predictions were increased by less blue and more green reflectance in early July. This combined use
598 of blue and green bands indicated increasing topsoil H with more productive vegetation on wetter
599 soils. In summary, the dominant pattern identified by the model was between high-low ground
600 (Bushnell, 1943; Sommer et al., 2008), but the degree of topsoil thinning or thickening was predicted
601 by the vegetation's response to soil conditions.

602 Cubist selected a much simpler combination of only DTA predictors to directly model the topsoil
603 SOC_{stock}. In general, the model predicted increasing SOC_{stock} with decreasing vertical distance to
604 channel. Areas low in relative elevation (1,100 m a-scale) and not far above the channel network
605 were predicted to have the largest SOC_{stock}. However, for areas low in relative elevation, but
606 sufficiently above the DEM based channel network, the model predicted the opposite trend of the
607 SOC_{stock} *decreasing* with decreasing vertical distance to channel. This pattern identified by the model
608 may be explained by a corresponding pattern observed in the model for the topsoil H. In that model,

609 areas low in relative elevation (1,100 m a-scale) were predicted to have some of the thickest topsoil
610 stocks. However, within a few of those zones the modelled topsoil H decreased with decreasing
611 relative elevation and TPI. This trend in the observed data, as detected by Cubist, was potentially
612 caused by an eroding out of topsoil sediments closer to the center of drainageways. In which case,
613 the vertical distance to channel – used in the topsoil SOC_{stock} model - may have been more an
614 indicator of proximity to the channel than wetness; the threshold was only 0.5 m above the channel
615 modelled from the DEM. Predictors related to surface flow energy would have been expected to be
616 better predictors of this kind of process. However, the upslope drainage network for much of the
617 map area extended beyond the boundaries of the available data. Thus the use of local elevation data
618 may have been a better proxy in this case, compared to the predictors calculated from truncated
619 watersheds.

620 *4.1.3. Subsoil model predictors*

621 With the exception of SOC%, the subsoil models all used several predictors from Landsat.
622 Selection of Landsat predictors for subsoil models suggested that vegetation characteristics or
623 surface soil moisture at different times of the year indicated subsoil conditions. In contrast, the
624 subsoil SOC% model's complete dependence on DTA predictors suggested that soil property was
625 mostly related to hydrology and that vegetation had little response to or effect on the SOC content
626 in the subsoil.

627 An example of spectral predictors detecting vegetation characteristics that likely reflected
628 subsoil conditions was the subsoil SK model. All of the MLR equations were strongly influenced by
629 the predictors of stream power, catchment slope, or SAGA wetness index. However, the skeleton-SK
630 predictions were modified by green reflectance in June and additional Landsat predictors collected
631 at different times of the year that related to the vigor of the vegetation. The weaker or drier the
632 vegetation appeared, the higher the prediction of SK content in the subsoil. Assuming soil moisture
633 conditions did not reach detrimental levels that year, these patterns fit known relationships

634 between particle size, soil drainage, and timing to crop maturity (Day and Intalap, 1970; Rawls et al.,
635 1982).

636 The generated model for subsoil BD most likely utilized a relationship with soil moisture as
637 detected by spectral predictors. In all areas, the MLR equations decreased predictions of subsoil BD
638 with increasing reflectance in the blue and SWIR-1 bands along with increasing emission in the TIR
639 band. Increases in the normalized difference vegetation index (NDVI) were used to slightly increase
640 predictions of subsoil BD. The use of the NDVI to offset the decreasing BD predicted by the other
641 Landsat predictors suggested those variables were indicating soil moisture conditions. Locations that
642 are wetter due to surface runoff would have a greater potential for organic material to be
643 translocated deeper in the soil profile (Schaetzl, 1986; Schaetzl, 1990). Also, the association of
644 wetter environments with cooler temperatures and anaerobic conditions would also inhibit
645 decomposition (Gates, 1942; Krause et al., 1959; Frazier and Lee, 1971).

646 The subsoil SOC% model was different than the other subsoil models generated. Instead of
647 selecting spectral predictors, the subsoil SOC% model relied solely on DTA predictors. The model
648 predicted the highest subsoil SOC% on steeper mid-slopes. The pattern of increasing subsoil SOC%
649 from the upper to middle slope fit the landscape translocation model proposed by Sommer et al.
650 (2000). In that study, the SOC% in the Bh horizon increased from the upper slope to the midslope due
651 to lateral translocation. Different than the pattern identified in the present study, the data in
652 Sommer et al. (2000) showed a continued increase in the SOC% of Bh horizons in the downslope
653 position. However, this contradiction may be partially explained by aggradation where the slope
654 gradient declines and the topsoil stock has been overthickened by developmental upbuilding
655 (McDonald and Busacca, 1990; Almond and Tonkin, 1999). Also, lateral flow would be expected to
656 return closer to the surface at downslope positions. In Sommer et al. (2000), while the upslope and
657 midslope profiles had E horizons separating the Bh from A horizons, the downslope Bh horizons
658 were exceptionally thick with little to no division between them and the A horizon. In that situation,

659 the definition of topsoil used in the present study would have grouped the downslope Bh horizons
660 into the topsoil stock. Therefore, the Cubist generated model may have been a simplification of the
661 complex interaction between topography and lateral flow depth and direction.

662 The rule groups for subsoil SOC% also differentiated for the plan curvature where the slope
663 gradient was not too high and the stream power index (SPI) was not too low. Concave plan
664 curvatures (138 m a-scale) were predicted to have increasingly higher and convex plan curvatures
665 were predicted to have increasingly lower subsoil SOC%. This relationship with plan curvature
666 matches patterns of water movement identified to be important to soil formation by Huggett (1975),
667 where convergent footslopes have the highest deposition rates (Pennock and De Jong, 1987).
668 Assuming the absence of any restrictive layer below, areas with the highest sediment deposition
669 rates would be expected to also have the highest volume of water infiltration.

670 The Cubist generated model for predicting the subsoil SOC_{stock} was simpler than any of the
671 indirect component models. It used only one MLR equation to relate red and infrared predictors to
672 subsoil SOC_{stock}. This model predicted more SOC_{stock} storage with increasing reflectance in the red
673 and SWIR-2 bands along with increasing emission in the TIR band – primarily captured on 6 July. Of
674 these variables, model predictions were dominated by increasing reflectance in the red band
675 increasing the estimated subsoil SOC_{stock}. This suggested less productive vegetation corresponding
676 with larger subsoil SOC_{stock}. This trend was counter to the patterns observed in the topsoil models,
677 but was sensible in the context of how the subsoil stock was defined for this study. Although the
678 total SOC_{stock} was less in areas with lower plant productivity, the subsoil SOC_{stock} was larger relative
679 to other subsoil areas due to the inverse relationship between topsoil and subsoil H used in this
680 study. A thicker topsoil stock would mean a thinner subsoil stock – and vice versa – due to the 2 m
681 depth limit. Regarding the other predictors in this model, increases in SWIR-2 reflectance could have
682 indicated more plant productivity. However, its use with the TIR band suggested that together they
683 were indicators of wetter soil conditions.

684 4.2. *Unconventional predictor selections*

685 The Cubist software made some intriguing selections in regards to predictors that were
686 calculated using alternative approaches. One example of this was the selection of alternative types
687 of aspect predictors. The conversion of aspect to northness and eastness is generally considered to
688 be the preferred method for addressing the circular problem of using aspect as a predictor. In our
689 approach of including many different predictors in the available pool, we also experimented with
690 simply rotating the central angle (position of 0°) to each cardinal direction for creating different
691 aspect predictors. In the models generated for this study, northness and eastness were only selected
692 for the topsoil SOC% model. In contrast, rotated versions of aspect were selected for the topsoil
693 SOC%, topsoil BD, as well as the topsoil and subsoil SK models.

694 Another example of an intriguing predictor selection by Cubist was the use of bands from the
695 LandsatLook products. These images were limited to four bands (SWIR-1, NIR, red, and TIR) and
696 were smoothed by an algorithm to facilitate image selection and visual interpretation. Although the
697 USGS does not recommend the use of these files for data analysis, the Cubist data mining found
698 them to be more useful than the data without LandsatLook processing. Most of these selections can
699 be explained by the greater variety of LandsatLook dates provided in the predictor pool. However,
700 there were a few instances where Cubist chose LandsatLook data over the unprocessed version of
701 the same Landsat data.

702 4.3. *Error propagation*

703 Although both the direct and indirect modelling approaches had base maps with a 2 m
704 resolution available to them, the direct modelling approach produced a more generalized SOC_{stock}
705 map. In terms of predicted error, the cost of trying to account for the variation in all of the variables
706 related to the SOC_{stock} appeared to be larger relative errors. The SOC_{stock} model from the direct
707 approach, on the other hand, did not attempt to predict as many variations occurring at small

708 phenomenon scales. Because these very local variations were difficult to predict, the estimated error
709 for the direct approach was less than for the indirect approach for most of the map area. Therefore,
710 it may be appropriate to consider the direct modelling approach to be a conservative approach for
711 estimating the SOC_{stock} for landscapes.

712 Possible sources of error in the base maps included atmospheric conditions for the satellite data
713 and the estimation of bare earth elevation under dense vegetation for the DEM. Several spectral
714 capture dates were made available in the predictor pool to enable Cubist to not only select the
715 optimal changes in seasonal vegetation characteristics, but to also select the image with minimal
716 noise from atmospheric effects such as clouds. Fewer options were available for DTA predictors,
717 because all DTA predictors needed to be derived from the same high-resolution DEM. The effect of
718 anomalies in the elevation data was more pronounced for larger a-scales. For example, a small forest
719 plot – located roughly between the two larger cities in the center of the map area – had not been
720 fully filtered out by the bare-earth algorithm. Any DTA calculation that included this area in its
721 analysis neighborhood was incorrectly influenced by those elevation values. The impact on this
722 study's models was an increased prediction of SOC_{stock} in the surrounding area.

723 The error propagation method used in this study could not directly account for errors in the base
724 maps. Instead, it could only quantify the combined model, base map, and target variable error
725 observed at sample locations. Although none of the sample points were in proximity to the before
726 mentioned error in the DEM, this phenomenon of elevation error affecting scale-dependent
727 predictors would have applied universally, even where the error was less obvious. The higher
728 relative error for both mapping approaches in the area surrounding the known problem in the DEM
729 suggested this potential source of error was at least partially accounted for.

730 **5. Conclusions**

731 This study demonstrated the use of spatial association to predict the SOC_{stock} and the estimated
732 error at unsampled locations within a 122 km² landscape at a high-resolution. The Cubist data

733 mining software detected patterns in the observed soil data, which was used to predict soil
734 properties in the greater map region. The ability of the available base maps to predict the variation
735 of those soil properties was quantified for each conditional rule of the respective models. The spatial
736 characteristics of the model rules allowed the uncertainty to be mapped along with the target
737 variable prediction.

738 There were two main advantages to using data mining software to produce relatively simple
739 model structures. First, patterns between the predictors and target variables were objectively
740 identified. Second, the resulting models were simple enough to be interpreted by the user and
741 related to known processes in the soil system. A relationship between selected predictors and
742 known processes provided confidence that their use in the model was not coincidental. The
743 separate modelling of topsoil and subsoil stocks identified a general division between useful
744 predictors for predicting soil properties at different depths. The data mining in this study suggested
745 DTA predictors tend to be most useful for topsoil properties, while spectral characteristics of
746 vegetation and soil moisture tend to be more useful for indicating subsoil properties.

747 Direct and indirect approaches were tested for predicting the SOC_{stock} with the rule-based, MLR
748 spatial modelling method. Although the spatial patterns in the two maps were generally similar, the
749 indirect approach produced a map with more spatial variation. While attempting to account for
750 more sources of variability resulted in less estimated error for the topsoil (indirect MAE = 1.69, direct
751 MAE = 2.27), the indirect approach had a higher potential for error in the subsoil (indirect MAE =
752 2.75, direct MAE = 1.37). Because the direct approach accounts for less variation (topsoil: direct R² =
753 0.58, indirect R² = 0.73; subsoil: direct R² = 0.14, indirect R² = 0.34), but also results in a lower total
754 MAE (direct MAE = 3.64, indirect MAE = 4.44), it should be considered a more conservative
755 prediction of the SOC_{stock}'s spatial distribution. The choice of which approach is best will likely
756 depend on a given situation's need to prioritize the representation of spatial pattern or to minimize
757 estimated error.

758 **Acknowledgements**

759 Data used in this research was collected as part of the Preagro project, funded by the German
760 Federal Ministry of Education and Research (BMBF), under grant reference number 0339740/2. We
761 thank Carsten Hoffmann for his suggestions during the development of this study.

762 **References**

763 Adhikari, K., Kheir, R.B., Greve, M.B., and Greve, M.H.: Comparing kriging and regression approaches
764 for mapping soil clay content in a diverse Danish landscape, *Soil Science*, 178(9), 505-517,
765 doi:10.1097/SS.0000000000000013, 2013.

766 Almond, P.C. and Tonkin, P.J.: Pedogenesis by upbuilding in an extreme leaching and weathering
767 environment, and slow loess accretion, south Westland, New Zealand, *Geoderma*, 92(1-2), 1-
768 36, doi: 10.1016/S0016-7061(99)00016-6, 1999.

769 Angers, D.A. and Carter, M.R.: Aggregation and organic matter storage in cool, humid agricultural
770 soils, in: *Structure and Organic Matter Storage in Agricultural Soils*, Carter, M.R. and Stewart,
771 B.A. (Eds.), CRC Press, Boca Raton, 193-211, 1996.

772 Ashley, M.D. and Rea, J.: Seasonal vegetation differences from ERTS imagery, *Journal of American
773 Society of Photogrammetry*, 41(6), 713-719, 1975.

774 Bannari, A., Morin, D., Bonn, F., and Huete, A.R.: A review of vegetation indices, *Remote Sensing
775 Reviews*, 13(1-2), 95-120, doi:10.1080/02757259509532298, 1995.

776 Bartholic, J.F., Namken, L.N., and Wiegand, C.L.: Aerial thermal scanner to determine temperature of
777 soils and of crop canopies differing in water stress, *Agronomy Journal*, 64(5), 603-608, 1972.

778 Bartholomeus, H.M., Schaepman, M.E., Kooistra, L., Stevens, A., Hoogmoed, W.B., and Spaargaren,
779 O.S.P.: Spectral reflectance based indices for soil organic carbon quantification, *Geoderma*,
780 145(1-2), 28-36, doi:10.1016/j.geoderma.2008.01.010, 2008.

781 Batjes, N.H.: Total carbon and nitrogen in the soils of the world, *European Journal of Soil Science*, 47,
782 151-163, doi:10.1111/j.1365-2389.1996.tb01386.x, 1996.

783 Beaudette, D.E. and O'Geen, A.T.: Quantifying the aspect affect: an application of solar radiation
784 modeling for soil survey, *Soil Science Society of America Journal*, 73(4), 1345-1352, 2009.

785 Bowman, R.A., Reeder, J.D., and Wienhold, B.J.: Quantifying laboratory and field variability to assess
786 potential for carbon sequestration, *Communications in Soil Science and Plant Analysis*, 33(9-10),
787 1629-1642, doi:10.1081/CSS-120004304, 2002.

788 Brenning, A., Koszinski, S., and Sommer, M.: Geostatistical homogenization of soil conductivity across
789 field boundaries, *Geoderma*, 143, 254-260, doi:10.1016/j.geoderma.2007.11.007, 2008.

790 Bui, E.N., Henderson, B.L., and Viergever, K.: Knowledge discovery from models of soil properties
791 developed through data mining, *Ecological Modelling*, 191, 431-446,
792 doi:10.1016/j.ecolmodel.2005.05.021, 2006.

793 Bushnell, T.M.: Some aspects of the soil catena concept, *Soil Science Society Proceedings*, 7(C), 466-
794 476, 1943.

795 Cambardella, C.A., Moorman, T.B., Novak, J.M., Parkin, T.B., Karlen, D.L., Turco, R.F., and Konopka,
796 A.E.: Field-scale variability of soil properties in central Iowa soils, *Soil Science Society of
797 America*, 58, 1501-1511, doi:10.2136/sssaj1994.03615995005800050033x, 1994.

798 Carlson, T.N., Gilles, R.R., and Perry, E.M.: A method to make use of thermal infrared temperature
799 and NDVI measurements to infer surface soil water content and fractional vegetation cover,
800 *Remote Sensing Reviews*, 9(1-2), 161-173, doi:10.1080/02757259409532220, 1994.

801 Churchill, R.R.: Aspect-related differences in badlands slope morphology, Annals of the Association
802 of American Geographers, 71(3), 374-388, doi:10.1111/j.1467-8306.1981.tb01363.x, 1981.

803 Cuff, J.R.I.: Quantifying erosion-causing parameters in a New Zealand watershed, in: Soil
804 Conservation, El-Swaify, S.A., Moldenhauer, W.C., Lo, A. (Eds.), Soil Conservation Society of
805 America, Ankeny, 99-112, 1985.

806 Daughtry, C.S.T.: Discriminating crop residues from soil by shortwave infrared reflectance, Agronomy
807 Journal, 93, 125-131, doi:10.2134/agronj2001.931125x, 2001.

808 Day, A.D. and Intalap, S.: Some effects of soil moisture stress on the growth of wheat (*Triticum*
809 *aestivum* L. em Thell), Agronomy Journal, 62(1), 27-29,
810 doi:10.2134/agronj1970.00021962006200010009x, 1970.

811 European Commission: European Soil Database v2, European Soil Data Centre,
812 <http://eusoils.jrc.ec.europa.eu>, last access: 7 October 2014.

813 FAO/IIASA/ISRIC/ISSCAS/JRC: Harmonized World Soil Database (version 1.2), FAO, Rome, Italy and
814 IIASA, Laxenburg, Austria, 2012.

815 Frazier, B.E. and Lee, G.B.: Characteristics and classification of three Wisconsin Histosols, Soil Science
816 Society of America Journal, 35(5), 776-780, doi:10.2136/sssaj1971.03615995003500050040x,
817 1971.

818 Gates, F.C.: The bogs of northern lower Michigan, Ecological Monographs, 12, 216-254,
819 doi:10.2307/1943542, 1942.

820 GLCF: Global Land Cover Facility, University of Maryland, <http://glcf.umd.edu/data>, last access: 19
821 February 2014.

822 Goidts, E., Van Wesemael, B., and Crucifix, M.: Magnitude and sources of uncertainties in soil organic
823 carbon (SOC) stock assessments at various scales, European Journal of Soil Science, 60(5), 723-
824 739, doi:10.1111/j.1365-2389.2009.01157.x, 2009.

825 Gomez, C., Viscarra Rossel, R.A., and McBratney, A.B.: Soil organic carbon prediction by
826 hyperspectral remote sensing and field vis-NIR spectroscopy: An Australian case study,
827 Geoderma, 146(3-4), 403-411, doi:10.1016/j.geoderma.2008.06.011, 2008.

828 Goodman, L.A.: On the exact variance of products, Journal of the American Statistical Association,
829 55, 708-713, 1960.

830 Grace, J.: Understanding and managing the global carbon cycle, Journal of Ecology, 92(2), 189-202,
831 doi:10.1111/j.0022-0477.2004.00874.x, 2004.

832 Grimm, R., Behrens, T., Märker, M., and Elsenbeer, H.: Soil organic carbon concentrations and stocks
833 on Barro Colorado Island – digital soil mapping using random forests analysis, Geoderma,
834 146(1-2), 102-113, doi:10.1016/j.geoderma.2008.05.008, 2008.

835 Hatfield, J.L., Gitelson, A.A., Schepers, J.S., and Walthall, C.L.: Application of spectral remote sensing
836 for agronomic decisions, Agronomy Journal, 100(3), S-117 – S-131,
837 doi:10.2134/agronj2006.0370c, 2008.

838 Heilman, J.L., Kanemasu, E.T., Rosenberg, N.J., and Blad, B.L.: Thermal scanner measurement of
839 canopy temperatures to estimate evapotranspiration, Remote Sensing of Environment, 5(C),
840 137-145, doi:10.1016/0034-4257(76)90044-4, 1976.

841 Holmes, G., Hall, M., and Frank, E.: Generating rule sets from model trees, Advanced Topics in
842 Artificial Intelligence, Lecture Notes in Computer Science, 1747, 1-12, doi:10.1007/3-540-
843 46695-9_1, 1999.

844 Huete, A.R.: A soil-adjusted vegetation index (SAVI), *Remote Sensing of Environment*, 25, 295-309,
845 doi:10.1016/0034-4257(88)90106-X, 1988.

846 Huggett, R.J.: Soil landscape systems: a model of soil genesis, *Geoderma*, 13, 1-22,
847 doi:10.1016/0016-7061(75)90035-X, 1975.

848 Hunckler, R.V. and Schaetzl, R.J.: Spodosol development as affected by geomorphic aspect, Baraga
849 County, Michigan, *Soil Science Society of America Journal*, 61(4), 1105-1115,
850 doi:10.2136/sssaj1997.03615995006100040017x, 1997.

851 Jobbág, E.G. and Jackson, R.B.: The vertical distribution of soil organic carbon and its relation to
852 climate and vegetation, *Ecological Applications*, 10(2), 423-436, doi:10.1890/1051-
853 0761(2000)010[0423:TVDOSO]2.0.CO;2, 2000.

854 Johnson, D.L., Keller, E.A., and Rockwell, T.K.: Dynamic pedogenesis: new views on some key
855 concepts, and a model for interpreting quaternary soils, *Quaternary Research*, 33(3), 306-319,
856 doi:10.1016/0033-5894(90)90058-S, 1990.

857 Johnston, A.E., Poulton, P.R., and Coleman, K.: Soil organic matter: its importance in sustainable
858 agriculture and carbon dioxide fluxes, *Advances in Agronomy*, 101, 1-57, doi:10.1016/S0065-
859 2113(08)00801-8, 2009.

860 Johnston, C.A., Groffman, P., Breshears, D.D., Cardon, Z.G., Currie, W., Emanuel, W., Gaudinski, J.,
861 Jackson, R.B., Lajtha, K., Nadelhoffer, K., Nelson, D., Jr., Mac Post, W., Retallack, G., and
862 Wielopolski, L.: Carbon cycling in soil, *Frontiers in Ecology and the Environment*, 2(10), 522-528,
863 doi:10.2307/3868382, 2004.

864 Kay, B.D.: Soil structure and organic carbon: a review, in: *Soil Processes and the Carbon Cycle*, Lal, R.,
865 Kimble, J.M., Follett, R.F., and Stewart, B.A. (Eds.), CRC Press, Boca Raton, 169-197, 1998.

866 Kempen, B., Brus, D.J., and Stoorvogel, J.J.: Three-dimensional mapping of soil organic matter
867 content using soil type-specific depth functions, *Geoderma*, 162, 107-123,
868 doi:10.1016/j.geoderma.2011.01.010, 2011.

869 Kennedy, B.A.: Valley-side slopes and climate, in: *Geomorphology and Climate*, Derbyshire, E. (Ed.),
870 John Wiley, London, 171-201, 1976.

871 Khalil, M.I., Kiely, G., O'Brien, P., and Müller, C.: Organic carbon stocks in agricultural soils in Ireland
872 using combined empirical and GIS approaches, *Geoderma*, 193-195, 222-235,
873 doi:10.1016/j.geoderma.2012.10.005, 2013.

874 Königlich Preußische Geologische Landesanstalt: Geologische Karte von Preußen und benachbarten
875 Bundesstaaten, 1:25,000 (Geological Map of Prussia and adjacent Federal States, 1:25,000),
876 Landesamt f. Geologie und Bergwesen, Halle, Sachsen-Anhalt, Germany, Sheet Wulfen 4137,
877 1913a.

878 Königlich Preußische Geologische Landesanstalt: Geologische Karte von Preußen und benachbarten
879 Bundesstaaten, 1:25,000 (Geological Map of Prussia and adjacent Federal States, 1:25,000),
880 Landesamt f. Geologie und Bergwesen, Halle, Sachsen-Anhalt, Germany, Sheet Cöthen 4237,
881 1913b.

882 Krause, H.H., Rieger, S., and Wilde, S.A.: Soils and forest growth on different aspects in the Tanana
883 watershed of interior Alaska, *Ecology*, 40, 492-495, doi:10.2307/1929773, 1959.

884 Kravchenko, A.N., Robertson, G.P., Hao, X., and Bullock, D.G.: Management practice effects on
885 surface total carbon: differences in spatial variability patterns, *Agronomy Journal*, 98, 1559-
886 1568, doi:10.2134/agronj2006.0066, 2006a.

887 Kravchenko, A.N., Robertson, G.P., Snap, S.S., and Smucker, A.J.M.: Using information about spatial
888 variability to improve estimates of total soil carbon, *Agronomy Journal*, 98, 823-829,
889 doi:10.2134/agronj2005.0305, 2006b.

890 Ku, H.H.: Notes on the use of propagation of error formulas, *Journal of Research of the National
891 Bureau of Standards – C. Engineering and Instrumentation*, 70C(4), 263-273, 1966.

892 Kühn, J., Brenning, A., Wehrhan, M., Koszinski, S., and Sommer, M.: Interpretation of electrical
893 conductivity patterns by soil properties and geological maps for precision agriculture, *Precision
894 Agriculture*, 10, 490-507, doi:10.1007/s11119-008-9103-z, 2009.

895 Lal, R.: Soil carbon sequestration impacts on global climate change and food security, *Science*,
896 304(5677), 1623-1627, doi:10.1126/science.1097396, 2004.

897 Lacoste, M., Minasny, B., McBratney, A., Michot, D., Viaud, V., and Walter, C.: High resolution 3D
898 mapping of soil organic carbon in a heterogeneous agricultural landscape, *Geoderma*, 213, 296-
899 311, doi:10.1016/j.geoderma.2013.07.002, 2014.

900 Lemercier, B., Lacoste, M., Loum, M., and Walter, C.: Extrapolation at regional scale of local soil
901 knowledge using boosted classification trees: a two-step approach, *Geoderma*, 171-172, 75-84,
902 doi:10.1016/j.geoderma.2011.03.010, 2012.

903 Li, Z.L., Tang, R., Wan, Z., Bi, Y., Zhou, C., Tang, B., Yan, G., and Zhang, X.: A review of current
904 methodologies for regional evapotranspiration estimation from remotely sensed data, *Sensors*
905 9(5), 3801-3853, doi:10.3390/s90503801, 2009.

906 Liebens, J. and VanMolle, M.: Influence of estimation procedure on soil organic carbon stock
907 assessment in Flanders, Belgium, *Soil Use and Management*, 19(4), 364-371,
908 doi:10.1111/j.1475-2743.2003.tb00327.x, 2003.

909 Lobell, D.B. and Asner, G.P.: Moisture effects on soil reflectance, *Soil Science Society of America
910 Journal*, 66, 722-727, doi:10.2136/sssaj2002.7220, 2002.

911 Lowther, J.R., Smethurst, P.J., Carlyle, J.C., and Nambiar, E.K.S.: Methods for determining organic
912 carbon in podzolic sands, *Communications in Soil Science and Plant Analysis*, 21(5-6), 457-470,
913 doi:10.1080/00103629009368245, 1990.

914 Lufafa, A., Diédhiou, I., Samba, S.A.N., Séne, M., Khouma, M., Kizito, F., Dick, R.P., Dossa, E., and
915 Noller, J.S.: Carbon stocks and patterns in native shrub communities of Senegal's Peanut Basin,
916 *Geoderma*, 146, 75-82, doi:10.1016/j.geoderma.2008.05.024, 2008.

917 Malone, B.P., McBratney, A.B., and Minasny, B.: Empirical estimates of uncertainty for mapping
918 continuous depth functions of soil attributes, *Geoderma*, 160, 614-626,
919 doi:10.1016/j.geoderma.2010.11.013, 2011.

920 Mardia, K.V., Kent, J.T., and Bibby, J.M.: *Multivariate Analysis*, Academic Press, London, United
921 Kingdom, 521 pp., 1979.

922 Martin, M.P., Orton, T.G., Lacarce, E., Meersmans, J., Saby, N.P.A., Paroissien, J.B., Jolivet, C.,
923 Boulonne, L., and Arrouays, D.: Evaluation of modelling approaches for predicting the spatial
924 distribution of soil organic carbon stocks at the national scale, *Geoderma*, 223-225, 97-107,
925 doi:10.1016/j.geoderma.2014.01.005, 2014.

926 Martin, M.P., Wattenbach, M., Smith, P., Meersmans, J., Jolivet, C., Boulonne, L., and Arrouays, D.:
927 Spatial distribution of soil organic carbon stocks in France, *Biogeosciences*, 8, 1053-1065,
928 doi:10.5194/bg-8-1053-2011, 2011.

929 McBratney, A.B. and Pringle, M.J.: Estimating average and proportional variograms of soil properties
930 and their potential use in precision agriculture, *Precision Agriculture*, 1, 125-152,
931 doi:10.1023/A:1009995404447, 1999.

932 McDonald, E.V. and Busacca, A.J.: Record of pre-late Wisconsin giant floods in the Channeled
933 Scabland interpreted from loess deposits, *Geology*, 16, 728-731, doi:10.1130/0091-
934 7613(1988)0162.3.CO;2, 1988.

935 Meersmans, J., Van Wesemael, B., De Ridder, F., Fallas Dotti, M., De Baets, S., and Van Molle, M.:
936 Changes in organic carbon distribution with depth in agricultural soils in northern Belgium,
937 1960-2006, *Global Change Biology*, 15(11), 2739-2750, doi:10.1111/j.1365-2486.2009.01855.x,
938 2009.

939 Migdall, S., Bach, H., Bobert, J., Wehrhan, M., and Mauser, W.: Inversion of a canopy reflectance
940 model using hyperspectral imagery for monitoring wheat growth and estimating yield, *Precision
941 Agriculture*, 10, 508-524, doi:10.1007/s11119-009-9104-6, 2009.

942 Miller, B.A., Koszinski, S., Wehrhan, M., and Sommer, M., Impact of multi-scale predictor selection
943 for modeling soil properties, *Geoderma*, 239-240, 97-106,
944 doi:10.1016/j.geoderma.2014.09.018, 2015.

945 Minasny, B. and McBratney, A.B.: Regression rules as a tool for predicting soil properties from
946 infrared reflectance spectroscopy, *Chemometrics and Intelligent Laboratory Systems*, 94(1), 72-
947 79, doi:10.1016/j.chemolab.2008.06.003, 2008.

948 Minasny, B., McBratney, A.B., Malone, B.P., and Wheeler, I.: Digital mapping of soil carbon, *Advances
949 in Agronomy*, 118, 1-47, doi:10.1016/B978-0-12-405942-9.00001-3, 2013.

950 Mishra, U., Lal, R., Liu, D., and Van Meirvenne, M.: Predicting the spatial variation of the soil organic
951 carbon pool at a regional scale, *Soil Science Society of America Journal*, 74, 906-914,
952 doi:10.2136/sssaj2009.0158, 2010.

953 Moore, I.D., Grayson, R.B., and Ladson, A.R.: Digital terrain modelling: a review of hydrological,
954 geomorphological, and biological applications, *Hydrological Processes*, 5(1), 3-30,
955 doi:10.1002/hyp.3360050103, 1991.

956 Mulder, V.L., de Bruin, S., Schaepman, M.E., and Mayr, T.R.: The use of remote sensing in soil and
957 terrain mapping – a review, *Geoderma*, 162, 1-19, doi:10.1016/j.geoderma.2010.12.018, 2011.

958 Myneni, R.B., Hall, F.G., Sellers, P.J., and Marshak, A.L.: The interpretation of spectral vegetation
959 indexes, *IEEE Transactions on Geoscience and Remote Sensing*, 33(2), 481-486,
960 doi:10.1109/36.377948, 1995.

961 Neemann, W.: Bestimmung des Bodenerodierbarkeitsfaktors für winderosionsgefährdete Böden
962 Norddeutschlands (Determination of soil erodibility factors for wind-erosion endangered soils
963 in Northern Germany), *Geologisches Jahrbuch Reihe F*, 25, 131 pp., 1991.

964 Nyssen, J., Temesgen, H., Lemenih, M., Zenebe, A., Haregeweyn, N., and Haile, M.: Spatial and
965 temporal variation of soil organic carbon stocks in a lake retreat area of the Ethiopian Rift
966 Valley, *Geoderma*, 146, 261-268, doi:10.1016/j.geoderma.2008.06.007, 2008.

967 Orton, T.G., Pringle, M.J., Page, K.L., Dalal, R.C., and Bishop, T.F.A.: Spatial prediction of soil organic
968 carbon stock using a linear model of coregionalisation, *Geoderma*, 230-231, 119-130,
969 doi:10.1016/j.geoderma.2014.04.016, 2014.

970 Panda, D.K., Singh, R., Kundu, D.K., Chakraborty, H., and Kumar, A.: Improved estimation of soil
971 organic carbon storage uncertainty using first-order Taylor series approximation, *Soil Science
972 Society of America Journal*, 72, 1708-1710, doi:10.2136/sssaj2007.0242N, 2008.

973 Pennock, D.J. and De Jong, E.: The influence of slope curvature on soil erosion and deposition in
974 hummock terrain, *Soil Science*, 144(3), 209-217, doi:10.1097/00010694-198709000-00007,
975 1987.

976 Petropoulos, G., Carlson, T.N., Wooster, M.J., and Islam, S.: A review of Ts/VI remote sensing based
977 methods for the retrieval of land surface energy fluxes and soil surface moisture, *Progress in
978 Physical Geography*, 33(2), 224-250, doi:10.1177/0309133309338997, 2009.

979 Phachomphon, K., Dlamini, P., and Chaplot, V.: Estimating carbon stocks at a regional level using soil
980 information and easily accessible auxiliary variables, *Geoderma*, 155(3-4), 372-380,
981 doi:10.1016/j.geoderma.2009.12.020, 2010.

982 Phillips, J.D.: On the relations between complex systems and the factorial model of soil formation
983 (with discussion), *Geoderma*, 86, 1-21, doi:10.1016/S0016-7061(98)00054-8, 1998.

984 Powlson, D.S., Whitmore, A.P., and Goulding, K.W.T.: Soil carbon sequestration to mitigate climate
985 change: a critical re-examination to identify the true and the false, *European Journal of Soil
986 Science*, 62, 42-55, doi:10.1111/j.1365-2389.2010.01342.x, 2011.

987 Quinlan, J.R. Learning with continuous classes, *Proceedings of the 5th Australian Joint Conference on
988 Artificial Intelligence*, 343-348, 1992.

989 Quinlan, J.R.: Combining instance-based and model-based learning, in: *Proceedings of the Tenth
990 International Conference on Machine Learning*, Kaufmann, M. (Ed.), 236-243, 1993.

991 Quinlan, J.R.: C4.5: Programs for machine learning, *Machine Learning*, 16, 235-240, 1994.

992 Rasmussen, M.S.: Developing simple, operational, consistent NDVI-vegetation models by applying
993 environmental and climatic information: Part I. Assessment of net primary production,
994 *International Journal of Remote Sensing*, 19(1), 97-117, doi:10.1080/014311698216459, 1998.

995 Rawls, W.J., Brakensiek, D.L., and Saxton, K.E.: Estimation of soil water properties, *Transactions of
996 the American Society of Agricultural Engineers*, 25(5), 1316-1320, 1982.

997 Rawls, W.J., Pachepsky, Y.A., Ritchie, J.C., Sobecki, T.M., and Bloodworth, H.: Effect of soil organic
998 carbon on soil water retention, *Geoderma*, 116(1-2), 61-76, doi:10.1016/S0016-7061(03)00094-
999 6, 2003.

1000 Richards, J.A.: *Remote Sensing Digital Image Analysis*, Springer, 439 pp., 2006.

1001 Richter, D.D. and Markewitz, D.: How deep is soil?, *Bioscience*, 45(9), 600-609, doi:10.2307/1312764,
1002 1995.

1003 Schaetzl, R.J.: Complete soil profile inversion by tree uprooting, *Physical Geography*, 7(2), 181-189,
1004 doi:10.1080/02723646.1986.10642290, 1986.

1005 Schrumpf, M., Schulze, E.D., Kaiser, K., and Schumacher, J.: How accurately can soil organic carbon
1006 stocks and stock changes be quantified by soil inventories?, *Biogeosciences*, 8(5), 1193-1212,
1007 doi:10.5194/bg-8-1193-2011, 2011.

1008 Schwartz, D. and Namri, M.: Mapping the total organic carbon in the soils of the Congo, *Global and*
1009 *Planetary Change*, 33(1-2), 77-93, doi:10.1016/S0921-8181(02)00063-2, 2002.

1010 Selige, S., Böhner, J., and Schmidhalter, U.: High resolution topsoil mapping using hyperspectral
1011 image and field data in multivariate regression modeling procedures, *Geoderma*, 136(1-2), 235-
1012 244, doi:10.1016/j.geoderma.2006.03.050, 2006.

1013 Simbahani, G.C., Dobermann, A., Goovaerts, P., Ping, J., and Haddix, L.: Fine-resolution mapping of
1014 soil organic carbon based on multivariate secondary data, *Geoderma*, 132, 471-489,
1015 doi:10.1016/j.geoderma.2005.07.001, 2006.

1016 Snyder, V.A. and Vazquez, M.A.: Structure, in: *Encyclopedia of Soils in the Environment*, Hillel, D.,
1017 Hatfield, J.L., Powlson, D.S., Rozenweig, C., Scow, K.M., Singer, M.J., and Sparks, D.L. (Eds.),
1018 Elsevier Academic Press, 54-68, 2005.

1019 Shrestha, D.L. and Solomatine, D.P.: Machine learning approaches for estimation of prediction
1020 interval for the model output, *Neural Networks*, 19(2), 225-235,
1021 doi:10.1016/j.neunet.2006.01.012, 2006.

1022 Sombroek, W.G., Fearnside, P.M., and Cravo, M.: Geographic assessment of carbon stored in
1023 Amazonian terrestrial ecosystems and their soils in particular, in: *Global Climate Change and*
1024 *Tropical Ecosystems*, Lal, R., Kimble, J.M., and Stewart, B.A. (Eds.), CRC Lewis, Boca Raton, 375-
1025 389, 2000.

1026 Sommer, M., Gerke, H.H., and Deumlich, D.: Modelling soil landscape genesis – a “time split”
1027 approach for hummocky agricultural landscapes, *Geoderma*, 145, 480-493,
1028 doi:10.1016/j.geoderma.2008.01.012, 2008.

1029 Sommer, M., Halm, D., Weller, U., Zarei, M., and Stahr, K.: Lateral podzolization in a granite
1030 landscape, *Soil Science Society of America Journal*, 64(4), 1434-1442,
1031 doi:10.2136/sssaj2000.6441434x, 2000.

1032 Soon, Y.K. and Abboud, S.: A comparison of some methods for soil organic carbon determination,
1033 *Communications in Soil Science and Plant Analysis*, 22(9-10), 943-954, doi:
1034 10.1080/00103629109368465, 1991.

1035 Stevens, A., Udelhoven, T., Denis, A., Tychon, B., Lioy, R., Hoffmann, L., and van Wesemael, B.:
1036 Measuring soil organic carbon in croplands at regional scale using airborne imaging
1037 spectroscopy, *Geoderma*, 158(1-2), 32-45, doi:10.1016/j.geoderma.2009.11.032, 2010.

1038 Sutherland, R.A.: Loss-on-ignition estimates of organic matter and relationships to organic carbon in
1039 fluvial sediments, *Hydrobiologia*, 389(1-3), 153-167, doi: 10.1023/A:1003570219018, 1998.

1040 Taylor, J.R.: *An Introduction to Error Analysis: The Study of Uncertainties in Physical Measurements*,
1041 2nd ed. University Science Books, Sausalito, California, USA, 1997.

1042 Ungaro, F., Staffilani, F., and Tarocco, P.: Assessing and mapping topsoil organic carbon stock at
1043 regional scale: a scorpan kriging approach conditional on soil map delineations and land use,
1044 Land Degradation & Development, 21, 565-581, doi:10.1002/lde.998, 2010.

1045 USGS: Earth Explorer, U.S. Geological Survey, <http://earthexplorer.usgs.gov>, last access 19 February
1046 2014.

1047 Walter, C., Viscarra Rossel, R.A., and McBratney, A.B.: Spatio-temporal simulation of the field-scale
1048 evolution of organic carbon over the landscape, Soil Science Society of America Journal, 67,
1049 1477-1486, doi:10.2136/sssaj2003.1477, 2003.

1050 Weaver, A. van Breda, The distribution of soil erosion as a function of slope aspect and parent
1051 material in Ciskei, Southern Africa, GeoJournal, 23(1), 29-34, doi:10.1007/BF00204406, 1991.

1052 Weisstein, E.W.: Error Propagation, Wolfram MathWorld,
1053 <http://mathworld.wolfram.com/ErrorPropagation.html>, last access: 25 August 2014.

1054 Wilhelm, W.W., Johnson, J.M.F., Hatfield, J.L., Voorhees, W.B., and Linden, D.R.: Crop and soil
1055 productivity response to corn residue removal: a literature review, Agronomy Journal, 96, 1-17,
1056 doi:10.2134/agronj2004.1000, 2004.

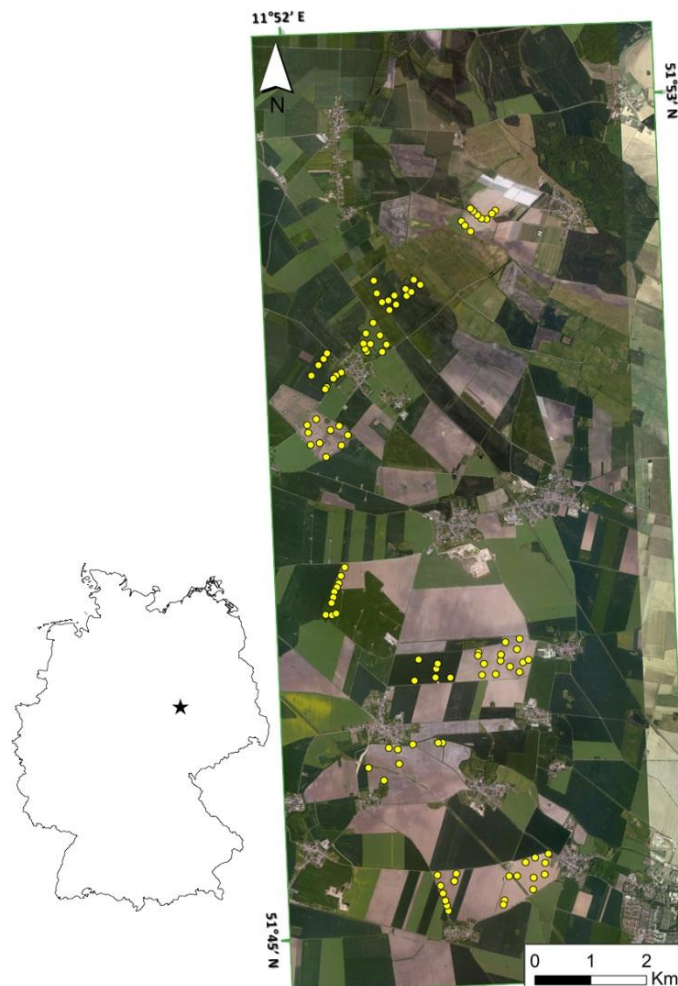
1057 Wilson, J.P. and Gallant, J.C. (Eds.): Terrain Analysis: Principles and Applications, John Wiley & Sons,
1058 2000.

1059 Xie, Y., Sha, Z., and Yu, M.: Remote sensing imagery in vegetation mapping: a review. Journal of Plant
1060 Ecology, 1(1), 9-23, doi:10.1093/jpe/rtm005, 2008.

1061 Zevenbergen, L.W. and Thorne, C.R.: Quantitative analysis of land surface topography, Earth Surface
1062 Processes and Landforms, 12(1), 47-56, doi:10.1002/esp.3290120107, 1987.

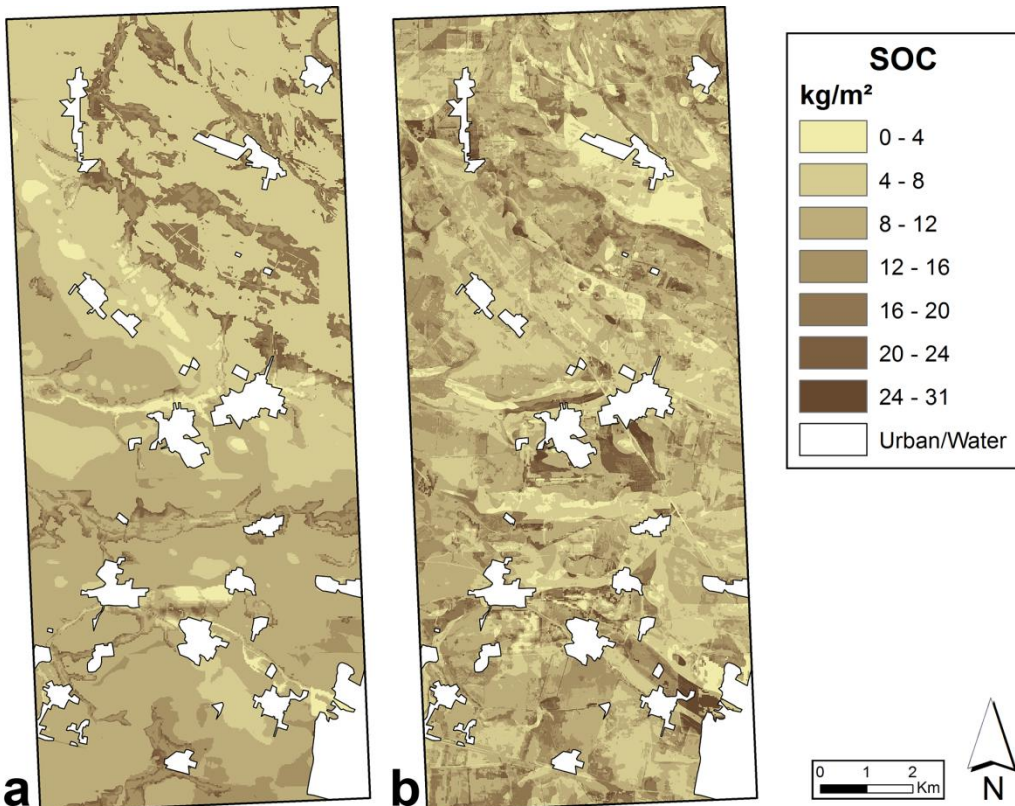
1063 Zhang, Z., Yu, D., Shi, X., Warner, E., Ren, H., Sun, W., Tan, M., and Wang, H.: Application of
1064 categorical information in the spatial prediction of soil organic carbon in the red soil area of
1065 China, Soil Science and Plant Nutrition, 56, 307-318, doi:10.1111/j.1747-0765.2010.00457.x,
1066 2010.

1067 Figures



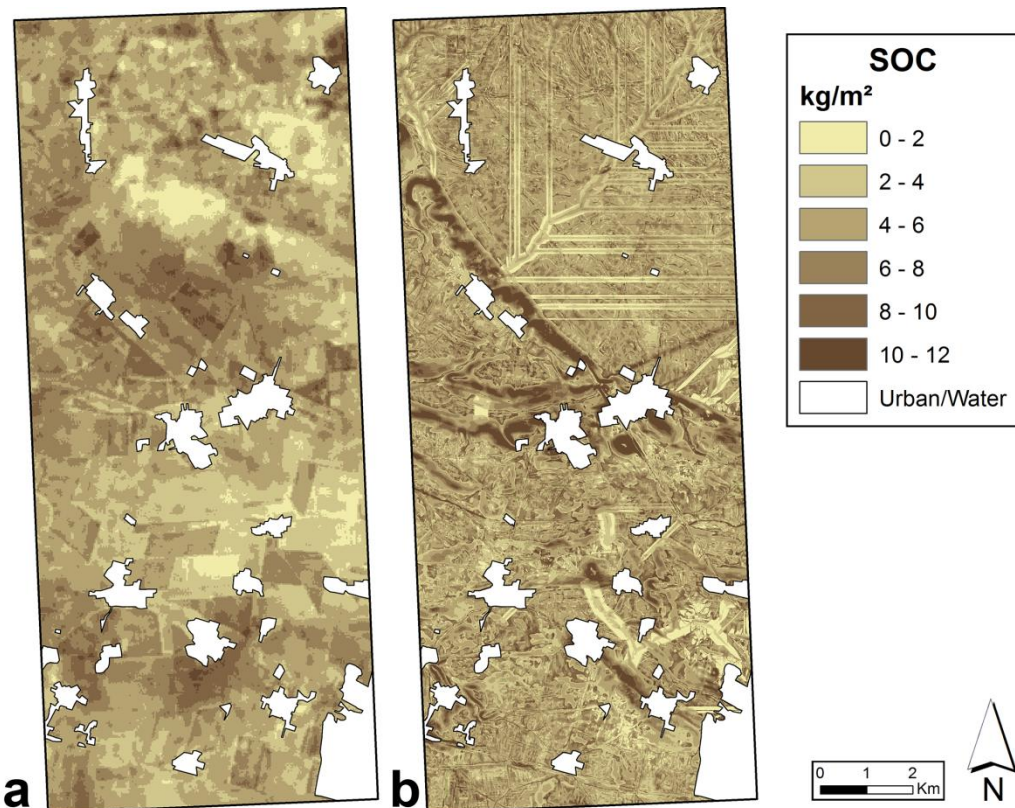
1068
1069

Figure 1. Locations of sample points and study area within Germany.



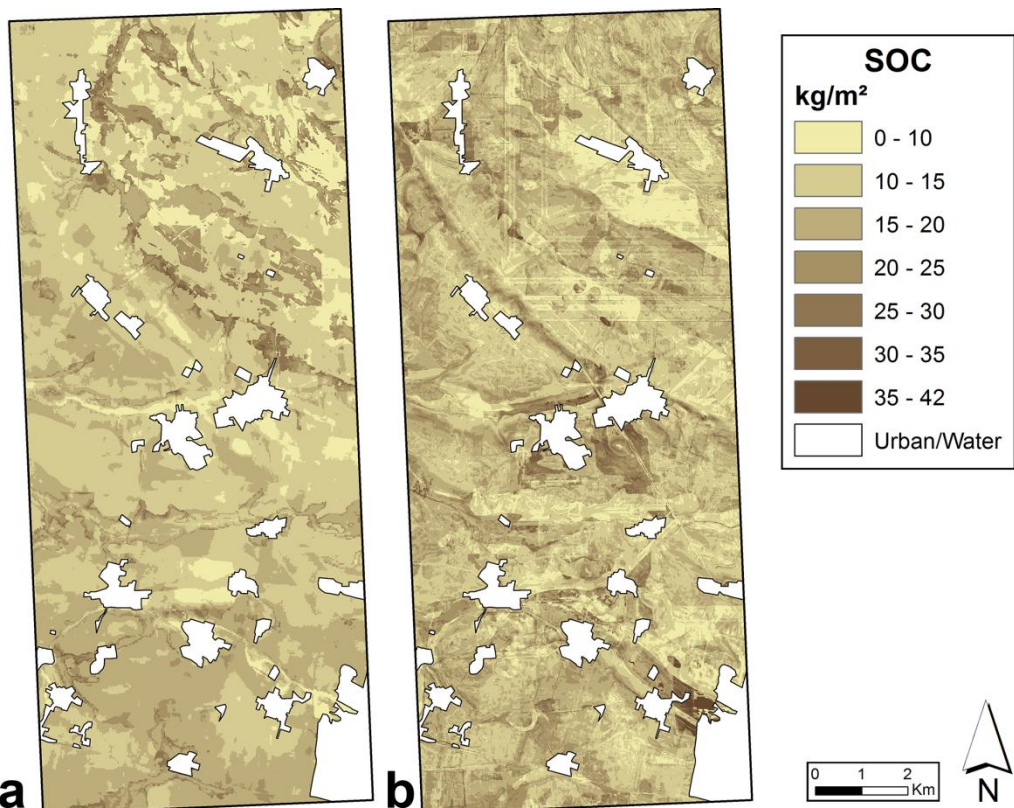
1070
1071
1072

Figure 2. Topsoil SOC_{stock} modelled by a) the direct approach and b) the indirect approach. Overlaid on a hillshade to show relationship with relief and field boundaries.

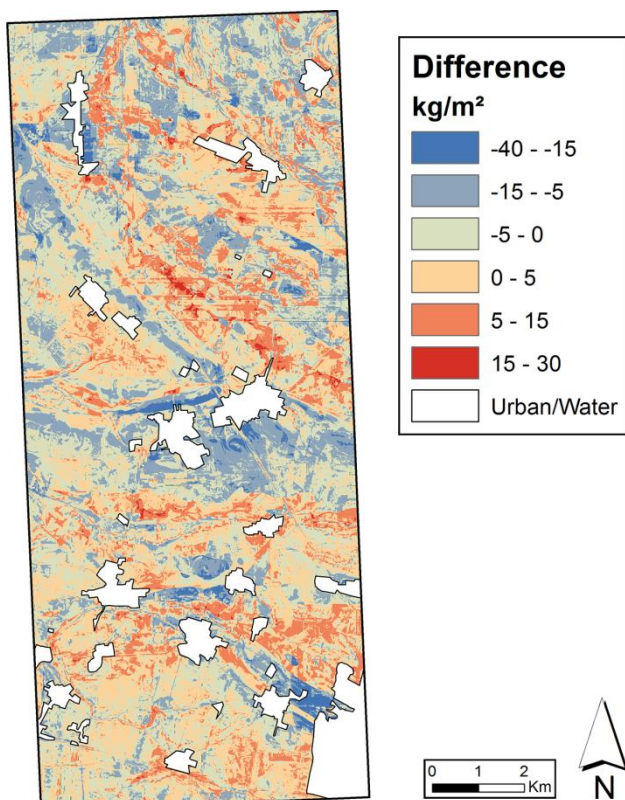


1073
1074
1075

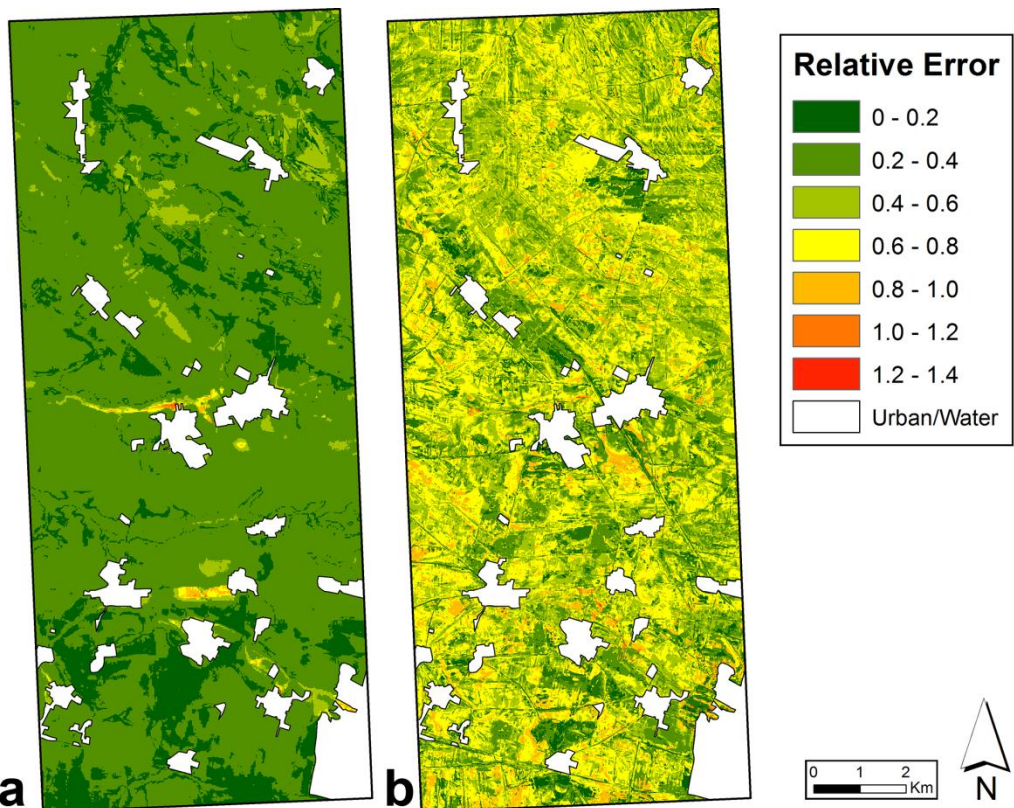
Figure 3. Subsoil SOC_{stock} modelled by a) the direct approach and b) the indirect approach. Overlaid on a hillshade to show relationship with relief and field boundaries.



1076
1077 Figure 4. Total SOC_{stock} (topsoil + subsoil) modelled by a) the direct approach and b) the indirect
1078 approach. Overlaid on a hillshade to show relationship with relief and field boundaries.



1079
1080 Figure 5. Calculated difference between the direct and indirect approaches of modelling the total
1081 SOC_{stock}. Negative values are where the indirect approach predicted more SOC_{stock} than the direct
1082 approach and positive values are where the indirect approach predicted less.



1083
1084
1085

Figure 6. Estimated relative error for the total SOC_{stock} modelled by a) the direct approach and b) the indirect approach.

1086 Tables

1087 Table 1. Descriptive statistics for the observed target variables. BD = total bulk density (g cm⁻³), SK =
1088 particles > 2 mm (%), SOC_% = SOC concentration (%), H = stock thickness (cm), and SOC_{stock} = mass of
1089 organic carbon per unit area of soil (kg m⁻²).

Topsoil	BD	SK	H	SOC_%	SOC_{stock}
Min.	1.18	0.00	10	0.75	1.80
Median	1.50	1.30	40	1.46	9.27
Mean	1.51	3.15	43.61	1.56	9.82
Max.	1.85	44.70	105	4.03	28.03
Std. Dev.	0.11	5.50	15.35	0.53	4.49

Subsoil	BD	SK	H	SOC_%	SOC_{stock}
Min.	1.33	0.00	18	0.02	0.07
Median	1.63	4.07	86	0.23	3.10
Mean	1.63	8.99	86.66	0.26	3.37
Max.	1.96	63.36	155	0.71	9.86
Std. Dev.	0.13	12.28	32.60	0.13	2.04

1090

1091 Table 2. Predictor variables considered in this study.

Predictor	Software	Analysis Scale
Elevation (LiDAR, bare-earth)	n/a	2 m
Slope gradient	GRASS	6 - 195 m
Profile curvature	GRASS	6 - 195 m
Plan curvature	GRASS	6 - 195 m
Aspect -west {rotated for N, E, and S}	GRASS	6 - 345 m
Aspect (8 classes)	ArcGIS (raster calculator)	6 - 345 m
Northness	transformed from aspect	6 - 345 m
Eastness	transformed from aspect	6 - 345 m
Longitudinal curvature	SAGA	10 m
Cross-section curvature	SAGA	10 m
Convexity	SAGA	10 m
Relative elevation - rect. neighborhood	ArcGIS toolbox	6 - 4000 m
Relative elevation - circ. neighborhood	ArcGIS toolbox	6 - 4000 m
Topographic position index (TPI)	ArcGIS toolbox	6 - 4000 m
TPI - slope position	ArcGIS toolbox	multiple
TPI - landform classification	ArcGIS toolbox	multiple
Hillslope position	ArcGIS toolbox	multiple
Catchment area	SAGA	n/a
Catchment slope	SAGA	n/a
Channel network base level	SAGA	n/a
Convergence index	SAGA	n/a
Flow accumulation	SAGA	n/a
Flow path length	SAGA	n/a
Length-slope factor	SAGA	n/a
Modified catchment area	SAGA	n/a
Relative slope position	SAGA	n/a
SAGA wetness index	SAGA	n/a
Stream power	SAGA	n/a
Vertical distance to channel	SAGA	n/a
Wetness index	SAGA	n/a
Geology (1:25,000 legacy map)	n/a	423 ha (mean)

1092

1093 Table 2 (cont'd).

Predictor	Resolution	Date
AVIS - LAI-green leaf area	5m	21 Jun. 2005
AVIS - LAI-brown leaf area	5m	21 Jun. 2005
Ikonos	4 m, 4 bands	4 Jul. 2006
Ikonos - panchromatic	1 m	4 Jul. 2006
Ikonos - LAI	5m	4 Jul. 2006
Ikonos - dry matter	5m	4 Jul. 2006
Landsat 5 NDVI (USGS, 2014)	30m	11 Jun. 2006
Landsat 5 NDVI (USGS, 2014)	30m	22 Jul. 2006
Landsat 5 LandsatLook (USGS, 2014)	30m, 3+1 band	20 Jun. 2006
Landsat 5 LandsatLook (USGS, 2014)	30m, 3+1 band	6 Jul. 2006
Landsat 5 LandsatLook (USGS, 2014)	30m, 3+1 band	22 Jul. 2006
Landsat 5 LandsatLook (USGS, 2014)	30m, 3+1 band	15 Sep. 2006
Landsat 5 LandsatLook (USGS, 2014)	30m, 3+1 band	17 Oct. 2006
Landsat 5 TM (USGS, 2014)	30m, 6 bands; 60m, 1 band	11 Jun. 2006
Landsat 5 TM (USGS, 2014)	30m, 6 bands; 60m, 1 band	22 Jul. 2006
Landsat 5 SR (GLCF, 2014)	30m, 7+2 bands	11 Jun. 2006
Landsat 5 SR (GLCF, 2014)	30m, 7+2 bands	22 Jul. 2006

1094

1095 Table 3. Relative use (%) of predictors in models derived by Cubist for the topsoil and subsoil stocks.
 1096 BD = total bulk density (g cm^{-3}), SK = particles > 2 mm (%), SOC% = SOC concentration (%), H = stock
 1097 thickness (cm), and SOC_{stock} = mass of organic carbon per unit area of soil (kg m^{-2}).

Topsoil			Subsoil		
Rules	MLR	Predictor	Rules	MLR	Predictor
BD			BD		
100%	100%	Relative elev. - circ. (2000 m)	100%	0%	Geology map units
51%	100%	Landsat5 SR, band 7 (6 Jun. 2006)	68%	100%	LandsatLook, band 5 (6 Jul. 2006)
17%	100%	Relative elev. - rect. (20 m)		100%	Landsat5 NDVI (22 Jul. 2006)
	96%	LandsatLook, band 5 (17 Oct. 2006)		100%	LandsatLook, band 6 (6 Jul. 2006)
	87%	Relative elev. - rect. (10 m)		100%	Landsat5 TM, band 1 (11 Jun. 2006)
	87%	Aspect, N central angle (215 m)		68%	Landsat5 SR, band 7 (22 Jul. 2006)
	83%	Landsat5 SR, band 2 (6 Jun. 2006)		32%	Landsat5 SR, band QA (6 Jun. 2006)
	34%	SAGA wetness index		32%	Landsat5 SR, band 1 (22 Jul. 2006)
	13%	Relative elev. - circ. (800 m)		32%	Landsat5 SR, band 6 (22 Jul. 2006)
SK			SK		
100%	100%	TPI (70 m)	100%	3%	Stream power
94%	0%	Aspect class (70 m)	76%	76%	Landsat5 SR, band 2 (11 Jun. 2006)
39%	16%	Relative elev. - rect. (550 m)	21%	0%	Profile Curvature (118 m)
37%	14%	LandsatLook, band 6 (17 Oct. 2006)	15%	79%	Landsat5 SR, band 4 (6 Jun. 2006)
	94%	Relative elev. - rect. (1800 m)		85%	Catchment slope
	84%	Landsat5 NDVI (11 Jun. 2006)		76%	LandsatLook, band 3 (20 Jun. 2006)
	80%	Aspect, N central angle (50 m)		56%	Landsat5 NDVI (11 Jun. 2006)
	78%	Landsat5 TM, band 4 (20 Jun. 2006)		56%	LandsatLook, band 4 (20 Jun. 2006)
	78%	Relative elev. - circ. (3000 m)		56%	Aspect, W central angle (70 m)
	64%	Aspect, N central angle (130 m)		21%	SAGA wetness index
	64%	Aspect, S central angle (345 m)			
	64%	Flow path length			
	37%	Aspect, N central angle (295 m)			
H			H		
100%	93%	Relative elev. - rect. (1100 m)			
39%	100%	LandsatLook, band 5 (15 Sept. 2006)			
34%	34%	LandsatLook, band 5 (22 Jul. 2006)			
25%	93%	Ikonos, band 2 (4 Jul. 2006)			
18%	7%	LandsatLook, band 4 (17 Oct. 2006)			
	100%	Relative elev. - rect. (1200 m)			
	93%	Ikonos, band 1 (4 Jul. 2006)			
	93%	Relative elev. - rect. (1300 m)			
	74%	LandsatLook, band 4 (15 Sept. 2006)			
	74%	TPI (1800 m)			
	74%	TPI (2600 m)			
	74%	Flow path length			
	28%	Relative elev. - circ. (650 m)			
	7%	Landsat5 TM, band 6 (11 Jun. 2006)			

1098

*Cubist not used
(based on 2 m - topsoil thickness)*

1099 Table 3 (cont'd).

Topsoil			Subsoil		
Rules	MLR	Predictor	Rules	MLR	Predictor
SOC%			SOC%		
100%	0%	Geology map units	100%	100%	Slope gradient (98 m)
49%	39%	Relative elev. - rect. (3200 m)	74%	74%	Stream power
39%	69%	Relative elev. - rect. (2000 m)	55%	55%	Plan curvature (138 m)
33%	74%	Flow path length	74%	74%	Slope gradient (90 m)
21%	62%	Northness (155 m)	74%	74%	Slope gradient (138 m)
81%	TPI (1200 m)		74%	74%	Slope gradient (185 m)
80%	Relative elev. - rect. (250 m)		74%	74%	Relative elev. - rect. (3400 m)
80%	Northness (345 m)		55%	55%	Plan curvature (90 m)
74%	Aspect, W central angle (90 m)		19%	19%	TPI (950 m)
69%	Relative elev. - circ. (1600 m)		19%	19%	Vertical distance to channel
69%	TPI (1100 m)				
62%	TPI (550 m)				
62%	Northness (215 m)				
62%	Eastness (345 m)				
62%	Modified catchment area				
32%	Aspect, W central angle (110 m)				
21%	TPI (250 m)				
21%	Aspect, W central angle (175 m)				
12%	Northness (6 m)				
SOC_{stock}			SOC_{stock}		
100%	48%	Relative elev. - rect. (1100 m)	100%	100%	LandsatLook, band 5 (6 Jul. 2006)
48%	100%	Vertical distance to channel	100%	100%	LandsatLook, band 3 (6 Jul. 2006)
80%	80%	Channel network base level	100%	100%	LandsatLook, band 6 (6 Jul. 2006)
			100%	100%	Landsat5 TM, band 7 (11 Jun. 2006)

1100

1101

1102 Table 4. Fitting performance for the respective models. The model's efficiency (ME) is the ratio
 1103 between the model's mean absolute error (MAE) and the MAE that would result from only using the
 1104 mean value as the model. Cubist reports the ME as relative error, but it is renamed here to avoid
 1105 confusion with the more common definition of relative error. An ME of greater than one indicates
 1106 that the model is not performing well.

Topsoil models	BD	SK	H	SOC%	Indirect - SOC _{stock}	Direct - SOC _{stock}
MAE	0.05	1.36	5.90	0.14	1.69	2.27
ME	0.52	0.41	0.47	0.34	0.49	0.66
R ²	0.69	0.85	0.71	0.86	0.73	0.58
Subsoil models						
MAE	0.06	3.77	5.90	0.06	2.75	1.37
ME	0.58	0.42	0.47	0.59	1.67	0.83
R ²	0.67	0.79	0.71	0.55	0.34	0.19

1107

1108 Table 5. Cross-validation performance for the respective models. Note that although the R^2 was
1109 severely reduced for most models, the MAE was generally only increased a small amount.

Topsoil models	BD	SK	H	SOC _%	Direct - SOC _{stock}
MAE	0.08	2.70	11.80	0.27	2.94
ME	0.86	0.82	0.93	0.66	0.85
R ²	0.26	0.08	0.12	0.61	0.27
Subsoil models					
MAE	0.09	7.18	11.80	0.09	1.42
ME	0.80	0.80	0.93	0.98	0.86
R ²	0.36	0.26	0.12	0.05	0.17

1110

1111 [Table 6. Skewness coefficients for the residuals of each model.](#)

	BD	SK	H	SOC _%	Indirect - SOC _{stock}	Direct - SOC _{stock}
Topsoil models	-0.25	-1.15	0.17	1.04	0.10	0.37
Subsoil models	0.11	-0.74	-0.17	1.18	-1.61	-0.16

1112